Journal of Structural Geology 112 (2018) 7–28

Contents lists available at ScienceDirect

Journal of Structural Geology

journal homepage: www.elsevier.com/locate/jsg

Review article

Brittle failure of rock: A review and general linear criterion

Joseph F. Labuz[a,*], Feitao Zeng[a,b], Roman Makhnenko[c], Yuan Li[d]

[a] Department of Civil, Environmental, and Geo- Engineering, University of Minnesota, Minneapolis, MN, USA
[b] Department of Engineering Mechanics, Dalian University of Technology, Dalian, Liaoning, China
[c] Department of Civil and Environmental Engineering, University of Illinois at Urbana-Champaign, IL, USA
[d] Department of Civil Engineering, University of Science and Technology Beijing, Beijing, China

ARTICLE INFO

Keywords:
Failure criteria
Failure surface
Friction angle
Intermediate stress effect
Multiaxial testing
Triaxial compression
Triaxial extension
True triaxial testing

ABSTRACT

A failure criterion typically is phenomenological since few models exist to theoretically derive the mathematical function. Indeed, a successful failure criterion is a generalization of experimental data obtained from strength tests on specimens subjected to known stress states. For isotropic rock that exhibits a pressure dependence on strength, a popular failure criterion is a linear equation in major and minor principal stresses, independent of the intermediate principal stress. A general linear failure criterion called Paul-Mohr-Coulomb (PMC) contains all three principal stresses with three material constants: friction angles for axisymmetric compression ϕ_c and extension ϕ_e and isotropic tensile strength V_o. PMC provides a framework to describe a nonlinear failure surface by a set of planes "hugging" the curved surface. Brittle failure of rock is reviewed and multiaxial test methods are summarized. Equations are presented to implement PMC for fitting strength data and determining the three material parameters. A piecewise linear approximation to a nonlinear failure surface is illustrated by fitting two planes with six material parameters to form either a 6- to 12-sided pyramid or a 6- to 12- to 6-sided pyramid. The particular nature of the failure surface is dictated by the experimental data.

1. Introduction

"The great tragedy of science – the slaying of a beautiful hypothesis by an ugly fact" (Huxley, 1870)

Rock is a challenging material to model but often times its mechanical response can be interpreted using theoretical approaches, *e.g.* to describe stiffness, or phenomenological approaches, *e.g.* to describe failure. With regard to stiffness, under certain loading conditions, rock can be modeled as a composite material of solids and voids, which can be further simplified as pores and cracks (Jaeger et al., 2007). Certainly the nature of the solids and voids is important; the collection of crystalline and amorphous particles of various size is affected by the mineralogy and cementing agent, and the voids' shape (pore-like and crack-like) and volume fraction (porosity n and crack density ρ) are critical in determining properties. However, in many ways, rock behaves in a similar manner from certain points of view. Thus, if the correct variables are used to evaluate experiments, then many phenomena can be explained by identical relations with different material parameters.

An example is the response of rock to the application of uniform stress (pressure), a loading arrangement that perfectly matches the assumed boundary condition, which is often not achieved in material testing. Fig. 1 illustrates the hydrostatic pressure – volumetric strain response of jacketed (the fluid is isolated from the rock) specimens of two quartz-rich sandstones, Dunnville (n = 30%) and Berea (n = 23%), along with fused quartz (Makhnenko and Labuz, 2016). Note that compression positive is used throughout the article. The initial nonlinear behavior for both sandstones is due to closing of crack-like voids, which are more prevalent for Berea. When sufficient pressure is achieved, approximately 25 MPa for the two sandstones, the response is linear (at pressures below yield). The slope of the linear portion gives effective bulk modulus K_{eff} = 10.7 GPa for Dunnville and K_{eff} = 12.1 GPa for Berea, basically due to the different amounts of porosity. Thus, upon crack closure both rocks behave in an elastic manner prior to yield and it can be shown that effective medium theories (Zimmerman, 1991; Kachanov, 1993) predict K_{eff}, knowing porosity and properties for solid quartz (K_s = 37.2 GPa, ν_s = 0.18).

Another example is the constitutive response of rock (Dunnville sandstone) under the stress states of uniaxial compression and tension (Fig. 2). Although the tests are simple in that only one stress component is nonzero, both uniaxial tests are challenging to the experimentalist because of frictional constraint and loading eccentricity, respectively. Uniaxial compression shows nonlinearity due to closing of some (not all) crack-like voids followed by a region of linearity, where isotropic

* Corresponding author.
E-mail address: jlabuz@umn.edu (J.F. Labuz).

https://doi.org/10.1016/j.jsg.2018.04.007
Received 14 October 2017; Received in revised form 21 March 2018; Accepted 6 April 2018
Available online 11 April 2018
0191-8141/

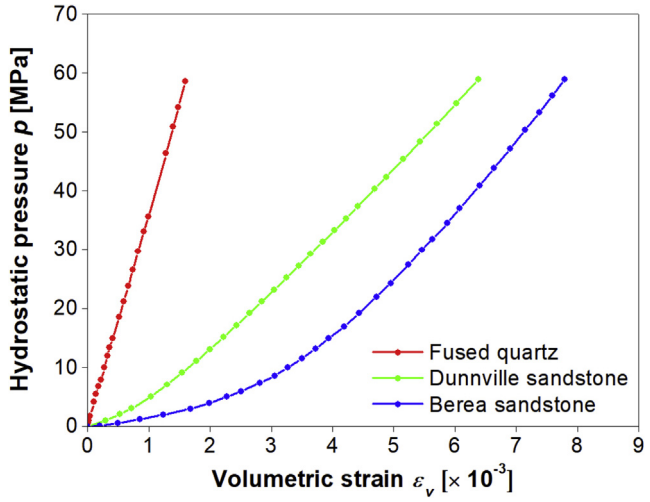

Fig. 1. Jacketed response of Dunnville sandstone, Berea sandstone, and fused quartz under hydrostatic loading.

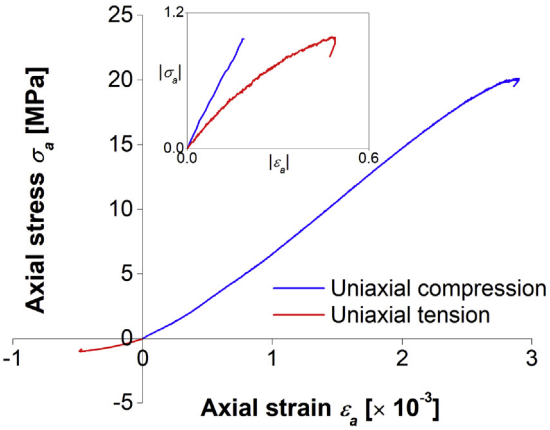

Fig. 2. Mechanical response of Dunnville sandstone under uniaxial compression and tension. The inset illustrates absolute values of axial stress and strain for the tension test and beginning of the compression test.

elasticity provides a basis for describing the material, with the effective Young's modulus E_{eff} = 8.4 GPa. Uniaxial tension shows linear response with E_{eff} = 2.8 GPa and it is clear that opening and sliding of crack-like voids are responsible for the softer response.

With continued loading beyond linear behavior where the yield stress is exceeded, the response shows nonlinearity (inelasticity), the details of which, *e.g.*, slip at grain boundaries or growth of existing cracks, are unimportant for developing a phenomenological model. The deformation process involves both reversible (elastic) and irreversible (plastic) strains. With continued deformation, a point of maximum or minimum (peak) stress is reached followed by a softening regime, where deformation has localized and strain is not homogeneous. Besides stiffness, a striking feature of rock-like materials under uniaxial loading is the order of magnitude contrast in the maximum and minimum axial stresses called uniaxial compressive strength (UCS or C_0) and uniaxial tensile strength (UTS or T). Indeed, the loading direction, *e.g.* uniaxial compression or tension (shortening or lengthening in only one direction), is a critical variable in describing failure.

The effect of pressure on the stress state at failure is illustrated in Fig. 3, the results from plane-strain compression testing (ε_{II} = 0, $\Delta\sigma_I > 0$, $\Delta\sigma_{III}$ = 0) of Red Wildmoor sandstone (Labuz et al., 2017). The notation $\sigma_I \geq \sigma_{II} \geq \sigma_{III}$ is used for the three principal stresses (and strains); volumetric strain $\varepsilon_v = \varepsilon_I + \varepsilon_{II} + \varepsilon_{III}$ and Δ denotes increment. The volumetric strain ε_v versus axial strain ε_I response shows linear

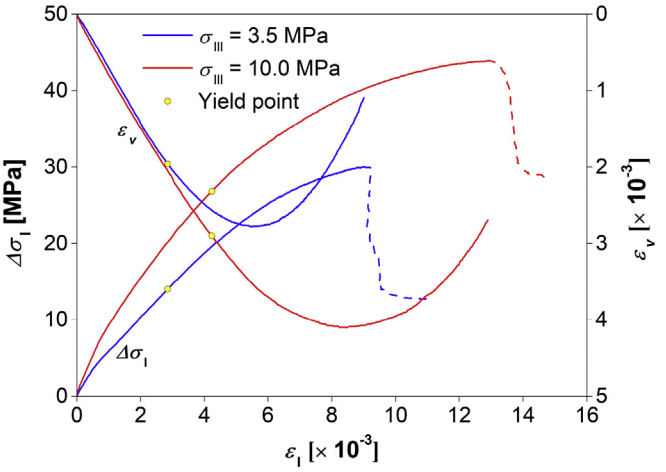

Fig. 3. Mechanical response of Red Wildmoor sandstone under plane-strain compression (Labuz et al., 2017).

elastic compaction, yield indicated by the deviation from linearity (dot in Fig. 3), and if the incremental elastic deformation is removed, plastic volume decrease (compaction) and/or plastic volume increase (dilation). The $\Delta\sigma_I - \varepsilon_I$ response features a linear part, yield (dot in Fig. 3), hardening with compaction and/or dilation, and peak stress. The post-peak response is shown with a broken curve because this is not constitutive; with localized deformation (fracture) appearing near peak stress, the softening response observed is due to not only material characteristics but also specimen size and specimen shape (Sture and Ko, 1978; Drescher and Vardoulakis, 1982; Labuz and Biolzi, 1991). These features – linearity, yield, hardening with plastic deformation, peak stress changing with confinement – are common for brittle response. Thus, an important characteristic that should be present in any failure criterion for rock in the brittle regime is increasing strength with increasing pressure, sometimes described as the frictional nature of rock.

The article reviews selected failure criteria for dry rock in the brittle regime and interprets experimental data to obtain material parameters that can be used to describe the stress state at failure. For saturated rock, stresses should be replaced by Terzaghi effective stresses. The term failure criteria, as opposed to yield criteria, is a more appropriate description of the objective. In the context of material behavior, failure is associated with a limiting stress called strength or a critical combination of stresses attaining a maximum value (*e.g.* maximum ratio of shear and normal tractions). Yield criteria and flow rules are features of plasticity theory. Although yielding indicates the start of inelastic (plastic) response, and for materials that do not harden, yield begins simultaneously with unrestricted plastic flow, failure criterion is the appropriate term to describe limiting stress, *i.e.* strength. Discussion is restricted to isotropic rock failing in a brittle manner, which means no yielding by application of pressure (Tarokh et al., 2017) and failure by a distinct fracture with an observable peak stress; further deformation occurs at decreasing stress. Details of the failure process involving natural deformation bands (localized failure) will not be considered (Aydin et al., 2006). Note that a brittle response can be changed to a ductile response by a sufficient increase in pressure (or temperature). The ductile failure mode, sometimes referred to as shear-enhanced compaction, is discussed by Wong and Baud (2012). Finally, a failure criterion should apply independent of rock type, from a soft limestone with UCS of a few MPa to a hard granite with UCS of several hundred MPa, although the quality and quantity of data may influence the interpretation.

2. Background

"… formulate the conditions of failure on a phenomenological ground…" (Nadai, 1950)

Most successful failure criteria are a generalization of experimental data obtained from a limited number of strength tests. Indeed, a failure criterion typically is conjectural since few models exist to theoretically derive the mathematical function, which is often assumed to be expressed in terms of stresses σ_{ij}:

$$f(\sigma_{xx}, \sigma_{yy}, \sigma_{zz}, \sigma_{xy}, \sigma_{yz}, \sigma_{zx}) = const \tag{1}$$

Significant efforts can be found in the literature on the selection of adequate forms of Eq. (1) and selected criteria are reviewed in Section 3.

For an isotropic material, whose strength properties are the same in all directions, the failure criterion must be a scalar function of the stress state and independent of the coordinate system. To satisfy this requirement, the failure criterion is written in terms of stress invariants, one option being the principal stresses σ_1, σ_2, σ_3 with no regard to order:

$$f(\sigma_1, \sigma_2, \sigma_3) = const \tag{2}$$

Other forms of a failure criterion include stress invariants that are particular combinations of the principal stresses:

$$f(I_1, J_2, J_3) = const \tag{3}$$

where I_1 is the first invariant of σ_{ij} and J_2 and J_3 are the second and third invariants of the deviator stress $S_{ij} = \sigma_{ij} - p\delta_{ij}$:

$$I_1 = \sigma_1 + \sigma_2 + \sigma_3 \tag{4}$$

$$J_2 = \frac{1}{6}[(\sigma_1 - \sigma_2)^2 + (\sigma_2 - \sigma_3)^2 + (\sigma_3 - \sigma_1)^2] \tag{5}$$

$$J_3 = (\sigma_1 - p)(\sigma_2 - p)(\sigma_3 - p) \tag{6}$$

Equivalently and used in this article, a failure criterion can be described by:

$$f(p, q, \theta) = const \tag{7}$$

where

$$p = \frac{I_1}{3} \tag{8}$$

$$q = \sqrt{3J_2} \tag{9}$$

$$\theta = \frac{1}{3}\arccos\left(\frac{3\sqrt{3}}{2}\frac{J_3}{J_2^{3/2}}\right) = \arctan\left(\frac{\sqrt{3}(\sigma_{II} - \sigma_{III})}{2\sigma_I - \sigma_{II} - \sigma_{III}}\right) \tag{10}$$

Note that the invariants p, q, θ have a physical and geometrical interpretation (Meldahl, 1944): p is hydrostatic or mean stress, q is shear stress intensity or deviatoric stress, and θ is the Lode angle, a measure of the stress state, where $0^\circ \le \theta \le 60^\circ$; *e.g.* $\theta = 0^\circ$ for axisymmetric compression ($\sigma_{II} = \sigma_{III}$) and $\theta = 60^\circ$ for axisymmetric extension ($\sigma_I = \sigma_{II}$). A failure criterion may contain one, two, or three principal stresses σ_I, σ_{II}, σ_{III} or one, two, or three stress invariants such as p, q, θ.

Eqs. (2), (3) and (7) describe a surface in principal stress space σ_1, σ_2, σ_3 called the failure surface, and because there are six possible orderings of the principal stresses: (i) $\sigma_1 \ge \sigma_3 \ge \sigma_2$, (ii) $\sigma_3 \ge \sigma_1 \ge \sigma_2$, (iii) $\sigma_3 \ge \sigma_2 \ge \sigma_1$, (iv) $\sigma_2 \ge \sigma_3 \ge \sigma_1$, (v) $\sigma_2 \ge \sigma_1 \ge \sigma_3$, and (vi) $\sigma_1 \ge \sigma_2 \ge \sigma_3$, Eq. (2) is actually six failure surfaces, each corresponding to a particular order of principal stresses. Fig. 4 is an example of a failure surface that is linear in principal stresses:

$$A\sigma_I + B\sigma_{II} + C\sigma_{III} = 1 \tag{11}$$

where A, B, C are material constants (Paul, 1968a,b). Note that material parameters are taken as positive quantities. The critical feature of pressure-dependence gives a pyramidal shape with a common vertex on the tension side of the hydrostatic axis, defined by $\sigma_1 = \sigma_2 = \sigma_3$. With $B = 0$, Eq. (11) describes the Mohr-Coulomb (MC) failure criterion. The surface representing the failure criterion defines the stress states associated with failure. Stress states outside the surface are inadmissible; stress states inside the surface are not at failure. The distance along the hydrostatic axis is related to p and the distance normal to the hydrostatic axis is related to q (Fig. 4a). Thus, the failure surface on the p, q plane shows the pressure dependence or frictional nature of rock.

Fig. 4b illustrates a section of the failure surface on a plane perpendicular to the hydrostatic axis called the equipressure or π-plane ($\sigma_1 + \sigma_2 + \sigma_3 = const$); the axes σ_1^*, σ_2^*, σ_3^* are the projections of the coordinate axes in the π-plane. This view displays the angle θ dependence and the distance along a θ-line is proportional to the deviatoric stress q. Clearly, for the failure surface shown in Fig. 4b, $q_c > q_e$, where q_c is the deviatoric stress for axisymmetric compression at $\theta = 0^\circ$ (also shown by solid lines at 120° and 240°) and q_e is the deviatoric stress for axisymmetric extension at $\theta = 60^\circ$ (also shown by dashed lines at 180° and 300°). Thus, for brittle failure of rock at the same mean stress, compression ($\sigma_{II} = \sigma_{III}$) failure is associated with a larger maximum shear stress compared to extension ($\sigma_{II} = \sigma_I$) failure. A failure surface with a circular cross-section on the π-plane, no θ dependence, displays a constant q (dashed circle in Fig. 4b) and this is only observed for porous rock under high mean stress (Wong and Baud, 2012).

For isotropic materials, the failure surface must display a three-fold symmetry and any one of the 60° sections uniquely defines the entire failure surface in the π-plane. It is often argued that the failure surface must be convex – each segment connecting two points within the region or on its boundary also belongs to this region or its boundary (Mroz, 1973). In addition, smoothness is a consideration with regard to the numerical implementation of a failure criterion (Willam and Warnke, 1975).

3. Review of failure criteria

"The history of our subject has been extremely well documented and surveyed at various intervals." (Paul, 1968b)

The mechanics literature contains a plethora of failure criteria and an extensive evaluation was provided by Yu (2002). Review will be limited to selected criteria through descriptions based on principal stresses (σ_I, σ_{II}, σ_{III}) or stress invariants (p, q, θ) and differences in failure criteria will be explained through the use of two or three variables and the mathematical functions, *e.g.* linear or nonlinear, that are used to capture the material behavior.

3.1. Criteria in terms of σ_I, σ_{III}

The popular Mohr-Coulomb (MC) failure criterion, $|\tau| = S_0 + \sigma tan\phi$, provides a reasonable approximation of strength over a limited range of normal stress, where σ and τ are normal and shear stresses on the failure plane, S_0 also known as cohesion c is the shear stress intercept on a Mohr (σ, τ) diagram, and ϕ is the internal friction angle. The linear equation in two principal stresses is

$$N\sigma_I - (N + 1)\sigma_{III} = V_0 \tag{12}$$

where $N = (1 - \sin\phi)/(2\sin\phi)$, V_0 = theoretical – it is not measured – isotropic tensile strength; $V_0\sin\phi = S_0\cos\phi$ and $C_0 = 2S_0\cos\phi/(1 - \sin\phi)$ is the uniaxial compressive strength. Note that failure criteria dependent on the major and minor principal stresses – the intermediate stress is ignored – can be displayed on the Mohr diagram of σ, τ. The circles representing the stress states at failure are uniquely defined by an envelope tangent to each circle. The failure surface is shown in Fig. 4, a six-sided pyramid in stress space (Fig. 4a) and an irregular hexagon in the π-plane (Fig. 4b). A severe limitation of MC is when one principal stress is tensile and a tension cut-off is needed (Paul, 1961).

It is known that the failure envelope is better represented as a curve rather than a straight line when the range of normal stress is large

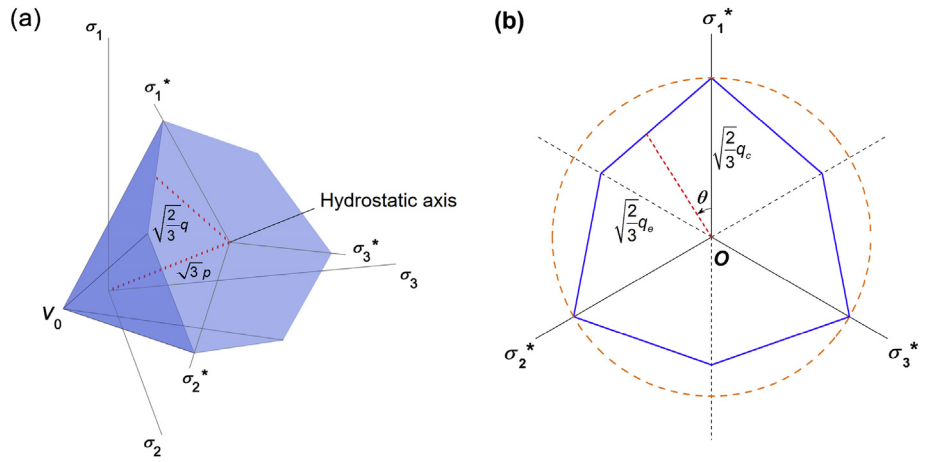

Fig. 4. Pyramidal failure surface in (a) principal stress space; (b) π-plane (dashed circle represents the failure surface of a cone).

(Jaeger et al., 2007). In order to capture the nonlinearity, a parabolic function was proposed by Fairhurst (1964):

$$\tau^2 = (m-1)^2 T(T+\sigma) \tag{13}$$

where T = uniaxial tensile strength, $m = (\eta + 1)^{1/2}$, and $\eta = C_0/T$. Transforming Eq. (13) to principal stresses, the failure criterion has a natural tension cut-off:

$$\begin{aligned} &-\sigma_{III} = T, \quad \sigma_I \le Tm(m-2) \\ &\frac{(\sigma_I-\sigma_{III})^2}{\sigma_I+\sigma_{III}} = 2(m-1)^2 T\left[1-\frac{2T}{\sigma_I+\sigma_{III}}\left\{\left(\frac{m-1}{2}\right)^2-1\right\}\right], \quad \sigma_I \ge Tm(m-2) \end{aligned} \tag{14}$$

Hoek and Brown (1980) proposed a criterion that takes the form

$$(\sigma_I-\sigma_{III})^2 = C_0^2\left(m_b\frac{\sigma_{III}}{C_0}+1\right) \tag{15}$$

where m_b is a fitting parameter. This criterion has been widely adopted by the rock mechanics community and parameter generalizations have been proposed (Hoek et al., 2002). A comparison of the three "σ_I -σ_{III} criteria" is shown in Fig. 5 for $C_0 = 30$ MPa, $T = 3$ MPa, $\phi = 34°$, $m_b = 10$. While the nonlinearity is apparent for both Fairhurst and Hoek-Brown in the σ_1,σ_3 plane (Fig. 5a), only slight nonlinearity appears in the π-plane for $p = 10$ MPa (Fig. 5b).

Other nonlinear equations have been suggested to capture the curved failure envelope, *e.g.* a parabolic function by Murrell (1965) and a power law by Hobbs (1970) and Pariseau (1994). A criterion represented by a nonlinear function of σ and τ can be rewritten in terms of σ_I and σ_{III} by applying the parametric transformation relations derived by Balmer (1952). Mogi (1971) proposed a criterion based on the octahedral shear stress $\tau_{oct} = \sqrt{2}q/3$ and a mean stress defined as $\sigma_{m,2} = (\sigma_I + \sigma_{III})/2$. The failure surface of Mogi can be either linear or nonlinear in the $\sigma_{m,2}$, τ_{oct} plane but it is curved in the π-plane (Al-Ajmi and Zimmerman, 2005). You (2009) introduced a Mogi-type criterion with exponential form, showing good agreement with some selected multiaxial strength data.

3.2. Criteria in terms of σ_I, σ_{II}, σ_{III}

MC can be written to include the intermediate stress σ_{II} and the result is Eq. (11), called Paul-Mohr-Coulomb (PMC) in honor of the researcher who proposed the failure criterion. Paul (1968a) identified the constants from the stress states of uniaxial compression, uniform triaxial (isotropic) tension, and uniaxial tension: $A = 1/C_0$, $B = -1/V_0 - 1/C_0 + 1/T_0$, $C = -1/T_0$, where C_0 = uniaxial compressive strength, T_0 = theoretical uniaxial tensile strength, and V_0 = theoretical isotropic tensile strength, the latter two not measured in experiments. Meyer and Labuz (2013) recast Eq. (11) in a form containing ϕ_c and ϕ_e, which are related to N_c and N_e:

$$N_c\sigma_I - (N_c - N_e)\sigma_{II} - (N_e+1)\sigma_{III} = V_0 \tag{16}$$

$$N_c = \left[\frac{1-\sin\phi_c}{2\sin\phi_c}\right], \quad N_e = \left[\frac{1-\sin\phi_e}{2\sin\phi_e}\right] \tag{17}$$

where ϕ_c is the friction angle in axisymmetric compression ($\sigma_{II} = \sigma_{III}$) and ϕ_e is the friction angle for axisymmetric extension ($\sigma_{II} = \sigma_I$). Others have noted the friction angle of rock to be dependent on stress state

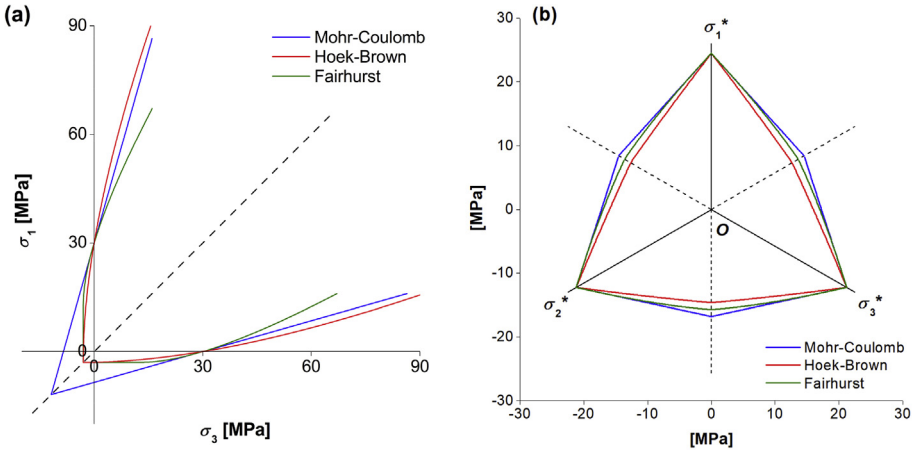

Fig. 5. Comparison of Mohr-Coulomb (MC), Fairhurst, Hoek-Brown (HB) failure criteria in the (a) σ_1,σ_3 plane; (b) π-plane.

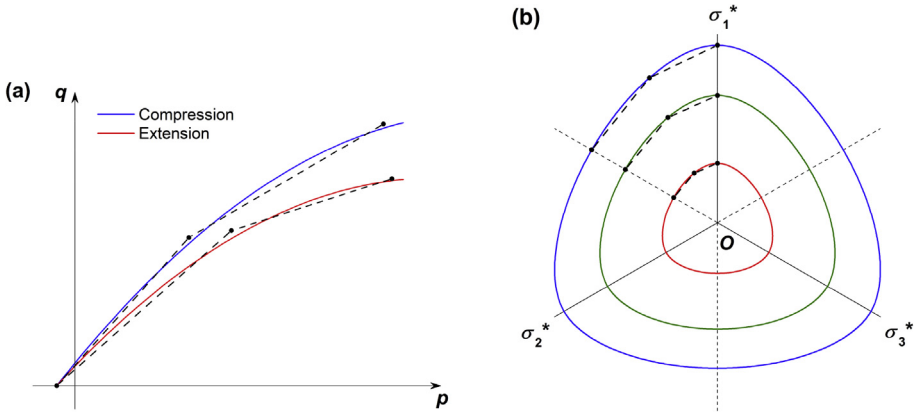

Fig. 6. Piecewise linear approximations to a nonlinear (Willam-Warnke) failure criterion in the (a) p, q plane; (b) π-plane.

(Topping, 1955; Haythornthwaite, 1962; Akai and Mori, 1967).

To account for the curved nature of a failure surface in a piecewise linear fashion in both the p, q plane and the π-plane, shown by the dashed lines in Fig. 6, two independent planes with six material parameters – four friction angles and two different vertices – can be fitted if sufficient data are available (Makhnenko et al., 2015; Zeng et al., 2018). Two planes describe the nonlinear failure surface in a piecewise linear manner, whereby the (i) mean stress dependence, (ii) θ effect, and (iii) changing shape on the π-plane are captured. The resulting failure surface is a six- and twelve-sided pyramid.

The failure surface of a circular cone (Schleicher, 1926; Nadai, 1950, 1933) can be written

$$\sqrt{(\sigma_{\mathrm{I}}-\sigma_{\mathrm{II}})^2+(\sigma_{\mathrm{II}}-\sigma_{\mathrm{III}})^2+(\sigma_{\mathrm{III}}-\sigma_{\mathrm{I}})^2}=A(\sigma_{\mathrm{I}}+\sigma_{\mathrm{II}}+\sigma_{\mathrm{III}})+B \tag{18}$$

which is smooth in the π-plane (shown by the dashed circle in Fig. 4b) and A and B are material parameters. Burzynski (1929) and Torre (1949) suggested the quadratic form (paraboloid of revolution) and Zhou (1994) called it the Modified Wiebols-Cook criterion. This smooth surface has advantages in numerical simulation, as a failure criterion containing corners in the π-plane does not have a unique gradient for defining the direction of the inelastic deformation (Borja, 2013). The orientation of the strain-increment vectors can be specified along the sides of the failure surface, but at corners in the π-plane, the direction is not unique. Several researchers have developed algorithms to handle corners (Ortiz and Popov, 1985; Sloan and Booker, 1986; De Borst, 1987; Runesson et al., 1988; Jeremić and Sture, 1997).

3.3. Criteria in terms of p, q, θ

Failure criteria written as functions of the three stress invariants p, q, θ readily display one, two, or three characteristics of rock failure in the brittle regime: (i) mean stress dependence, (ii) θ effect, (iii) changing shape on the π-plane. A circular failure surface on the π-plane (no θ effect) and linear in the p, q plane – the Schleicher-Nadai cone – was popularized by Drucker and Prager (1952) and can be written simply as

$$q=Ap+B \tag{19}$$

where, *e.g.* $A=(6\sin\phi)/(3-\sin\phi)$ and $B=(6V_0\sin\phi)/(3-\sin\phi)$ are the material parameters that fit MC at the compression corners (Fig. 4b). Nonlinear functions have been used to fit strength data in the p, q plane, an example of which is the expansion of the Hoek-Brown (HB) criterion; the failure surface in the π-plane changes to a circle, as opposed to that shown in Fig. 5b, and keeps the classical HB function in the p, q plane (Pan and Hudson, 1988; Priest, 2005).

The circular cross-section in the π-plane, Eq. (18) or (19), is not consistent with experimental data for brittle failure of rock. Thus, the stress invariant θ (or J_3) should be included in the failure criterion and some of the first investigators to do so were Cherry et al. (1968) and Wiebols and Cook (1968). Matsuoka and Nakai (1974) proposed a criterion based on the concept of a "spatial mobilized plane," postulating that failure takes place when the ratio between shear and normal stresses on a plane reaches a critical value. Lade and Duncan (1975) proposed a criterion for cohesionless soil and it was later modified by Lade (1977), Kim and Lade (1984), and Ewy (1999) for rock.

Willam and Warnke (1975) developed a notable criterion that is linear (three parameters) or quadratic (five parameters) in the p, q plane (Fig. 6a) with an elliptical and changing shape in the π-plane (Fig. 6b):

$$q=g_{ww}(\theta)\cdot q_c(p) \tag{20}$$

where $q_c(p)$ is the deviatoric stress for triaxial compression and $g_{ww}(\theta)$ is the shape function given by

$$g_{ww}(\theta)=\frac{2(1-\beta^2)\cos\left(\theta-\frac{\pi}{3}\right)+(2\beta-1)\sqrt{4(1-\beta^2)\cos^2\left(\theta-\frac{\pi}{3}\right)+5\beta^2-4\beta}}{4(1-\beta^2)\cos^2\left(\theta-\frac{\pi}{3}\right)+(2\beta-1)^2} \tag{21}$$

with $\beta=q_e/q_c$. Note that $g_{ww}(\theta)$ is unconditionally convex and smooth for the range $0.5\le\beta\le1$ due to its elliptical nature and it satisfies the conditions $g_{ww}(0)=1$ and $g_{ww}(\pi/3)=\beta$. If β is constant, $g_{ww}(\theta)$ is a function of only θ, which means that the corresponding failure surfaces in the π-plane do not change shape. If β is not constant and varies with p, $g_{ww}(\theta)$ is a function of both θ and p, which means that the shape of the failure surfaces in the π-plane change with p (Fig. 6b). A schematic representation of PMC with two planes is shown by the dashed lines in Fig. 6.

Ottosen (1977) suggested a four-parameter criterion that is nonlinear in the p, q and π-planes. A highlight of Ottosen's criterion is that the corresponding trace in the π-plane changes from triangular to more circular shape with increasing mean stress. Desai (1980) suggested using a complete polynomial function in terms of I_1, J_2, J_3. Hsieh et al. (1982) proposed a four-parameter criterion, which appears as a smooth curve in the p, q plane and triangular curved sections in the π-plane. Menetrey and Willam (1995) proposed a generalized criterion based on the HB criterion with a parabolic form. Similar to Ottosen's criterion, Menetrey-Willam failure surface is parabolic in the p, q plane while the π-plane shape changes from curved triangular at low mean stress to circular at high mean stress. Aubertin et al. (2000) developed a criterion with a nonlinear failure surface in the p, q plane and a parameter that controls the shape in the π-plane.

Zhang and Zhu (2007) modified the HB criterion by introducing a smooth transition between the triaxial compression and extension points in the π-plane and keeping the classical HB function in the p, q plane. Mortara (2008) provided a general formulation by adding a

parameter that controls the shape of failure surface in the π-plane and including a function to improve the data fitting in the p, q plane. Benz et al. (2008) extended HB by using the concepts from Matsuoka-Nakai. Du et al. (2010) proposed a nonlinear criterion capable of covering a curved triangle to a circle in the π-plane with an exponential curve in the p, q plane. Lee et al. (2012) formulated two criteria by combining the (1) MC criterion with the Jiang and Pietruszczak (1988) shape function and (2) HB criterion with the Willam-Warnke shape function. Rudnicki (2017) introduced a yield criterion as a modified and generalized form of Matsuoka-Nakai and Lade-Duncan. Rudnicki's approach provides a means to predict orientation of the failure plane through a bifurcation analysis.

In summary, it is convenient to generalize failure criteria by

$$q = f(p)g(\theta) \tag{22}$$

where $f(p)$ is associated with the mean stress dependence and $g(\theta)$, called the shape function, is associated with the θ (or J_3) effect and possibly shape change in the π-plane. Various forms of Eq. (22) have been suggested and are discussed by van Eekelen (1980), Podgorski (1985), Desai and Salami (1987), Rubin (1991), Labbane et al. (1993), Bigoni and Piccolroaz (2004), and Lagioia and Panteghini (2016). Other shape functions have been developed by Mills and Zimmerman (1970), Argyris et al. (1974), Haythornthwaite (1985), Boswell and Chen (1987), Bardet (1990), Krenk (1996), and the limits of the constants have been analyzed by Lin and Bažant (1986), Schreyer (1989), and Panteghini and Lagioia (2014).

4. Approaches for testing

> *"Demonstratio longe optima est experiential." By far the best proof is an experiment.* (Attributed to Sir Francis Bacon, from Harbottle, 1906)

The success of a failure criterion should be assessed using laboratory data from well controlled experiments called element tests, the objective of which is to produce a homogeneous stress state in a material specimen with static (traction prescribed) or kinematic (displacement prescribed) boundaries. In typical loading arrangements, lubricated surfaces are crucial for element testing to eliminate frictional constraint at the interface between the rock and end-pieces (platens). Well machined specimens to achieve frictionless kinematic boundaries, with no rotation, are fundamental in element testing.

A thorough presentation on apparatus for rock testing is found in Paterson and Wong (2005) and only highlights will be mentioned. An early study of rock strength under uniaxial and biaxial stress was conducted by Föppl (1900) where the use of *stearin* is reported, and stearic acid as a lubricant was revived by Labuz and Bridell (1993). von Kármán (1911) and Böker (1915) are often credited with the first axisymmetric or "triaxial" – two principal stresses are equal – compression and extension tests on rock using right circular cylinders (Fig. 7a), *i.e.* cores. Triaxial testing is performed by jacketing the specimen, placing it in a pressure vessel sometimes called a triaxial cell, and generating radial stress by fluid pressure, an ideal boundary condition. Axial stress is developed by a hydraulic or screw-driven load frame through platens in contact with the rock specimen and the issue of frictional constraint appears. Griggs (1936), Balmer (1953), Handin and Hager (1957), Heard (1960), Brace (1964), Paterson (1964), Murrell (1965), Donath (1966), Franklin and Hoek (1968) contributed significant efforts, basically following the pioneering work of von Kármán. Note that axisymmetric compression and extension tests offer simple approaches to evaluate an influence of the intermediate stress.

Recognizing the limitation of a conventional triaxial test – the three principal stresses cannot be varied independently – multiaxial devices became a pursuit. Kvapil and Luffer (1960), Dreyer and Borchert (1962), Akai and Mori (1967), Niwa and Kobayashi (1967), Niwa et al. (1967), Hojem and Cook (1968), Bieniawski et al. (1969), Mogi (1971), and Atkinson and Ko (1973) designed and built apparatus for "true triaxial" testing and others have followed. The basic concept involves loading a right rectangular prism (Fig. 7b) through static and/or kinematic boundaries, depending on the design. By their nature, a multiaxial apparatus is more complex mechanically than a triaxial device and jacketing of the specimen can be a significant challenge. Further, boundary conditions and specimen aspect ratios (height/width) play a more influential role because of frictional constraint and the failure plane intersecting the platens (Fig. 7b). Specimen size relative to a material length scale such as grain size is also a concern.

A particular stress state of interest is associated with the plane strain condition and several researchers have developed biaxial (2D) strain apparatus (Stavropoulou, 1982; Wawersik et al., 1990; Ord et al., 1991; Labuz et al., 1996). An advantage with a plane strain device is that deformation is enforced to be 2D and the failure plane forms in the σ_I, σ_{III} plane. Vardoulakis and Goldscheider (1981) recognized this feature and devised a clever approach (Fig. 7c) to monitor failure into the post-peak region: a linear bearing is mounted on the upper or lower platen and translation is allowed with no system interaction once the failure mechanism is formed. Ord et al. (1991) and Labuz et al. (1996) followed the Vardoulakis-Goldscheider approach and deformation characteristics of failure initiation and propagation can be studied (Riedel and Labuz, 2007).

Multiaxial devices are housed in research laboratories world-wide, *e.g.* Schwartzkopff et al. (2013) in Australia; Descamps et al. (2012) in Belgium; Young et al. (2013) in Canada; He et al. (2010) and Feng et al. (2016) in China; Bésuelle and Hall (2011) in France; Michelis (1985) in Greece; Mogi (2007) and Takahashi and Koide (1989) in Japan; Rukhaiyar and Samadhiya (2017) in India; Karev and Kovalenko (2013)

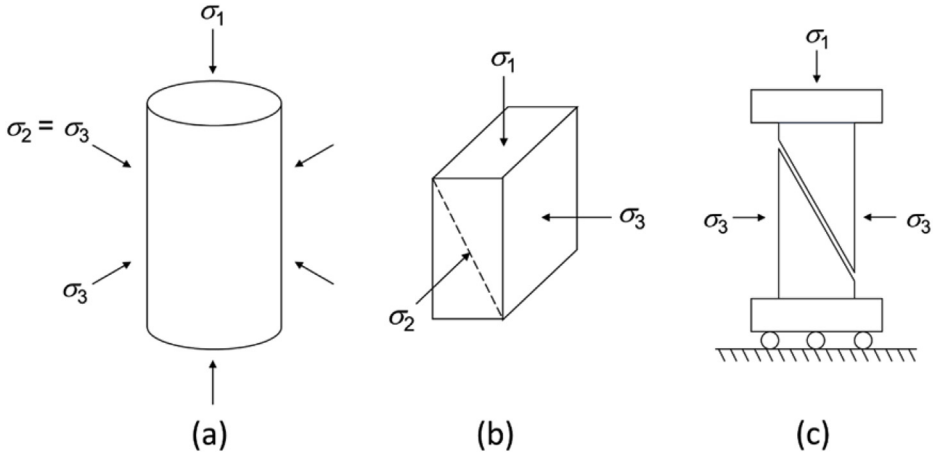

Fig. 7. Loading conditions for strength testing: (a) axisymmetric; (b) multiaxial; (c) plane-strain with no constraint.

in Russia; Kapang et al. (2013) in Thailand; King et al. (1995) in the UK; Alexeev et al. (2004) in Ukraine; Reches and Dieterich (1983), Wawersik et al. (1997) and Haimson and Chang (2000) in the US. A collection of papers from a workshop summarized the state of the practice (Kwaśniewski et al., 2013). Note that the majority of true triaxial tests have been conducted with constant σ_{II} and σ_{III}, with the exceptions of the work of Ingraham et al. (2013), where all three principal stresses were controlled in order to keep mean stress and Lode angle θ constant, and Ma et al. (2017), where tests were conducted to achieve constant θ but with changing mean stress.

5. Analysis of experiments with a linear criterion

> *"Because of the wide variety of possible failure surfaces, and the analytic complexities associated with many of them, it is logical to explore the simplifications which will result if we approximate a general nonlinear failure surface by an approximating surface which consists of a set of planes which hug the curved surface to any degree of accuracy desired."* (Paul, 1968a)

Based on experimental data, a failure criterion of rock should include (i) mean stress dependence, (ii) θ effect, and (iii) changing shape on the π-plane. In addition, the mathematical model of the failure surface should provide a close fit of the experimental data representing the failure mode of brittle fracture and identify model parameters with clear physical meaning and standard fitting methods. Other issues related to the mathematical description of the failure surface are convexity, which is typically satisfied by the fitting of the data, and smoothness. The nature of rock failure supports a gradual change in response for small variations in stress state and obviously a sharp corner of a general linear criterion does not provide a gradual change. Nonetheless, the smoothness condition and its derivatives being continuous are mathematical conveniences associated with a failure surface, and the simplest approach – the linear criterion of PMC – will be used to analyze strength experiments. A tension cut-off is needed when one or more of the principal stresses are tensile (Meyer and Labuz, 2013).

5.1. PMC with three parameters

To determine the three material parameters ϕ_c, ϕ_e, and V_0, an approach is proposed based on the transformation relations between principal stresses and p, q, θ. Fig. 8 is a sketch of PMC failure surface in the p, q plane for triaxial compression, triaxial extension, and multiaxial testing. Note that if $-q$ is used for extension, then the p, q plane is

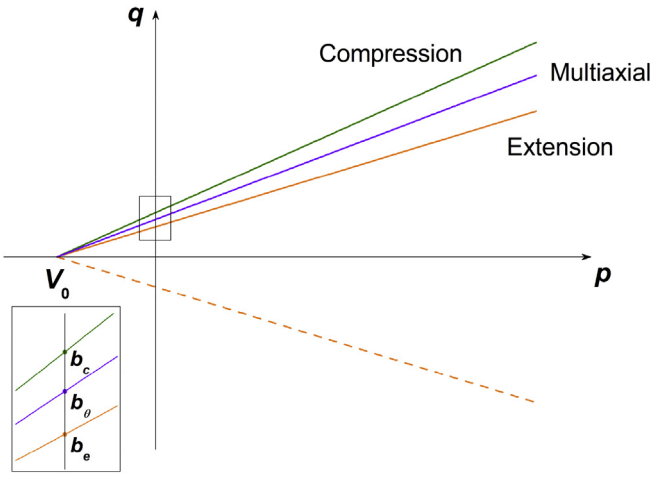

Fig. 8. Linear criterion in p, q plane for axisymmetric compression and extension, and multiaxial failure states; to represent the cross-section of the failure surface, $-q$ is used for extension.

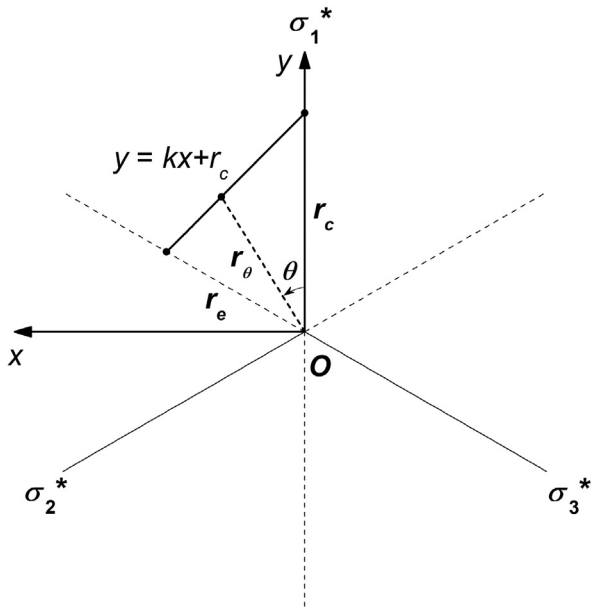

Fig. 9. Linear failure surface in the π-plane $p = 0$ with polar and Cartesian coordinate systems.

related to the cross-section of the failure surface in principal stress space containing σ_1^* and the hydrostatic axis $\sqrt{3}p$ (Fig. 4a). The compression, extension, and multiaxial lines intersect the q-axis at b_c, b_e, and b_θ, and the p-axis at V_0. Thus, the PMC failure criterion in the p, q plane can be reformulated as:

$$q = b_\theta\left(\frac{p}{V_0} + 1\right) \tag{23}$$

where q denotes the deviatoric stress at a particular θ.

Fig. 9 shows PMC in the π-plane for $p = 0$. Any stress state in the π-plane (p = const) can be represented by r_θ, θ in a polar coordinate system. The distance r_θ between the point representing the stress state in principal stress space and the hydrostatic axis is associated with q. The transformation relations between principal stresses and the r_θ, θ, p coordinate system are

$$\begin{aligned}\sigma_1 &= p + \tfrac{\sqrt{6}}{3} r_\theta \cos\theta \\ \sigma_2 &= p - \tfrac{\sqrt{6}}{3} r_\theta \sin\left(\tfrac{\pi}{6} - \theta\right) \\ \sigma_3 &= p - \tfrac{\sqrt{6}}{3} r_\theta \sin\left(\tfrac{\pi}{6} + \theta\right)\end{aligned} \tag{24}$$

At $p = 0$, the intercept b_θ and the distance r_θ can be written with respect to θ in the π-plane: when $\theta = 0^\circ$, $b_\theta = b_c$ and $r_\theta = r_c$; when $\theta = 60^\circ$, $b_\theta = b_e$ and $r_\theta = r_e$. The variation of b_θ with respect to θ within the range of 0°–60° shows the effect of the stress state.

In the π-plane (Fig. 9), the failure line $y = kx + r_c$ can be expressed by r_θ and θ:

$$r_\theta \cos\theta = k \cdot r_\theta \sin\theta + r_c \tag{25}$$

where k is the slope of the line in the π-plane. Solving Eq. (25) for r_θ gives

$$r_\theta = \frac{r_c}{\cos\theta - k\sin\theta} \tag{26}$$

It can be shown that the distance r_θ in any π-plane is related to q (Davis and Selvadurai, 2002):

$$r_\theta = \sqrt{\frac{2}{3}} \cdot q \tag{27}$$

Note that $q = b_\theta$ when $p = 0$, so Eq. (27) gives

$$r_\theta = \sqrt{\frac{2}{3}} \cdot b_\theta \tag{28}$$

Substituting Eq. (28) into Eq. (26) and simplifying, an expression for b_θ is obtained:

$$b_\theta = \frac{b_c}{\cos\theta - k \sin\theta} \tag{29}$$

Eq. (29) is the expression of the intercept b_θ in the p, q plane. Because the failure line goes through the axisymmetric extension point ($r_\theta = r_e$, $\theta = 60°$) in the π-plane, Eq. (25) becomes

$$r_e = \sqrt{3} \cdot k \cdot r_e + 2r_c \tag{30}$$

Considering Eq. (28), the ratio $\alpha = r_c/r_e$ can be written as

$$\alpha = \frac{r_c}{r_e} = \frac{\sqrt{\frac{2}{3}} \cdot b_c}{\sqrt{\frac{2}{3}} \cdot b_e} = \frac{b_c}{b_e} \tag{31}$$

Solving Eq. (30) for k and substituting Eq. (31) into Eq. (30) gives

$$k = \frac{1 - 2\alpha}{\sqrt{3}} \tag{32}$$

Knowing the expression for b_θ and k, the general equation of PMC, Eq. (23), is

$$\frac{b_c}{V_0} p + kq \sin\theta + b_c = q \cos\theta \tag{33}$$

From Eq. (33), a system of linear equations can be constructed using compression, extension, and multiaxial testing data. Strength experiments are typically associated with $\sigma_I^i, \sigma_{II}^i, \sigma_{III}^i$ and p_i, q_i, θ_i are calculated for each stress state. Thus, a system of linear equations is generated with the form $\mathbf{A}\cdot\mathbf{x} = \mathbf{b}$:

$$\begin{pmatrix} p_1 & q_1 \sin\theta_1 & 1 \\ p_2 & q_2 \sin\theta_2 & 1 \\ \vdots & \vdots & \vdots \\ p_n & q_n \sin\theta_n & 1 \end{pmatrix} \cdot \begin{pmatrix} b_c/V_0 \\ k \\ b_c \end{pmatrix} = \begin{pmatrix} q_1 \cos\theta_1 \\ q_2 \cos\theta_2 \\ \vdots \\ q_n \cos\theta_n \end{pmatrix} \tag{34}$$

where $\mathbf{A}$ = rectangular data matrix, $\mathbf{x}$ = parameter vector, and $\mathbf{b}$ = data vector. The least-squares method is used to solve Eq. (34) for b_c/V_0, k, and b_c; b_e is calculated from Eqs. (31) and (32). According to the expressions of compression and extension lines in the p, q plane, ϕ_c and ϕ_e are given by

$$\sin\phi_c = \frac{3b_c}{6V_0 + b_c} \tag{35}$$

$$\sin\phi_e = \frac{3b_e}{6V_0 - b_e} \tag{36}$$

Therefore, the three material parameters ϕ_c, ϕ_e, and V_0 can be determined.

To evaluate the three material parameters of PMC, experimental results from axisymmetric compression and extension tests are examined from previous studies: Darley Dale sandstone (Murrell, 1965), Red Wildmoor sandstone (Papamichos et al., 2000), Berea sandstone (Bobich, 2005), Apulian calcarenite (Meyer and Labuz, 2013), and Indiana limestone (Makhnenko and Labuz, 2014). For these data sets, the range of mean stress is not large – a nonlinear failure surface in the p, q plane is not apparent – and the three-parameter model (one plane) accurately describes the failure surface. Fig. 10 illustrates an example of the three-parameter fitting and data in the p, q plane for Red Wildmoor sandstone; for clarity of presentation, extension data are plotted as $-q$. The slope of the axisymmetric compression line is $(6\sin\phi_c)/(3 - \sin\phi_c)$ and the slope of the (negative) extension line is $-(6\sin\phi_e)/(3 + \sin\phi_e)$, with $\phi_c = 34.0°$ and $\phi_e = 41.5°$. Even though $\phi_e > \phi_c$, the slope of the extension line in the p, q plane usually is smaller than the compression line, as illustrated in Fig. 10; the slopes are equal for the Schleicher-Nadai cone.

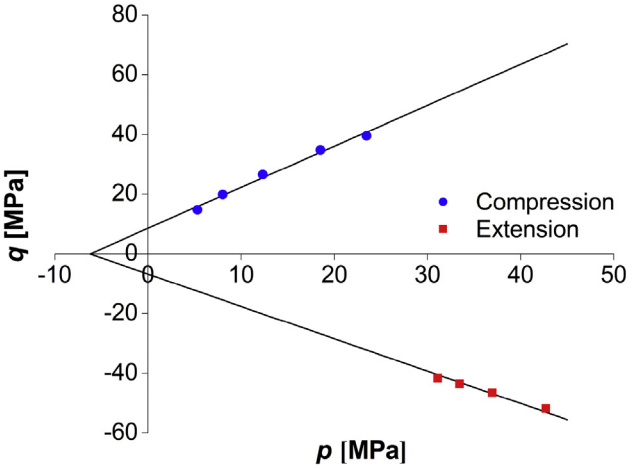

Fig. 10. PMC failure surface and data in the p, q plane from strength tests on Red Wildmoor sandstone (Papamichos et al., 2000); extension data are plotted as $-q$.

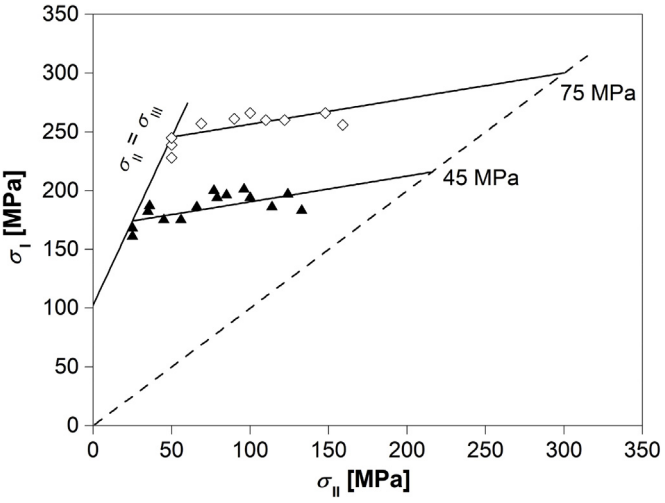

Fig. 11. PMC failure surface and data in the σ_I, σ_{II} plane from strength tests on Yuubari shale (Takahashi and Koide, 1989).

Strength data from multiaxial testing can be used in the fitting, *e.g.* Yuubari shale (Takahashi and Koide, 1989) and the experimental results can be shown in the σ_I, σ_{II} plane (Fig. 11). These data are well expressed by a linear relation so the three-parameter failure surface is appropriate. From Eq. (16), is it clear that (a) the failure lines at constant σ_{III} are parallel with a slope of $[1 - (N_e/N_c)]$ and (b) the axisymmetric compression line has a slope of $[1 + (1/N_c)]$. Table 1

Table 1
Values of the three PMC parameters for selected rock; see Tables A1–A6 for data.

Rock	Reference	ϕ_c (°)	ϕ_e (°)	V_0 (MPa)	R^2
Darley Dale sandstone	Murrell, 1965	34.3	37.6	44.7	0.99
Yuubari shale	Takahashi and Koide, 1989	28.8	32.9	55.3	0.96
Red Wildmoor sandstone	Papamichos et al., 2000	34.0	41.5	6.2	0.98
Berea sandstone	Bobich, 2005	37.7	44.2	21.7	0.98
Apulian calcarenite	Meyer and Labuz, 2013	21.6	22.6	13.6	0.99
Indiana limestone	Makhnenko and Labuz, 2014	29.3	30.2	26.4	0.97

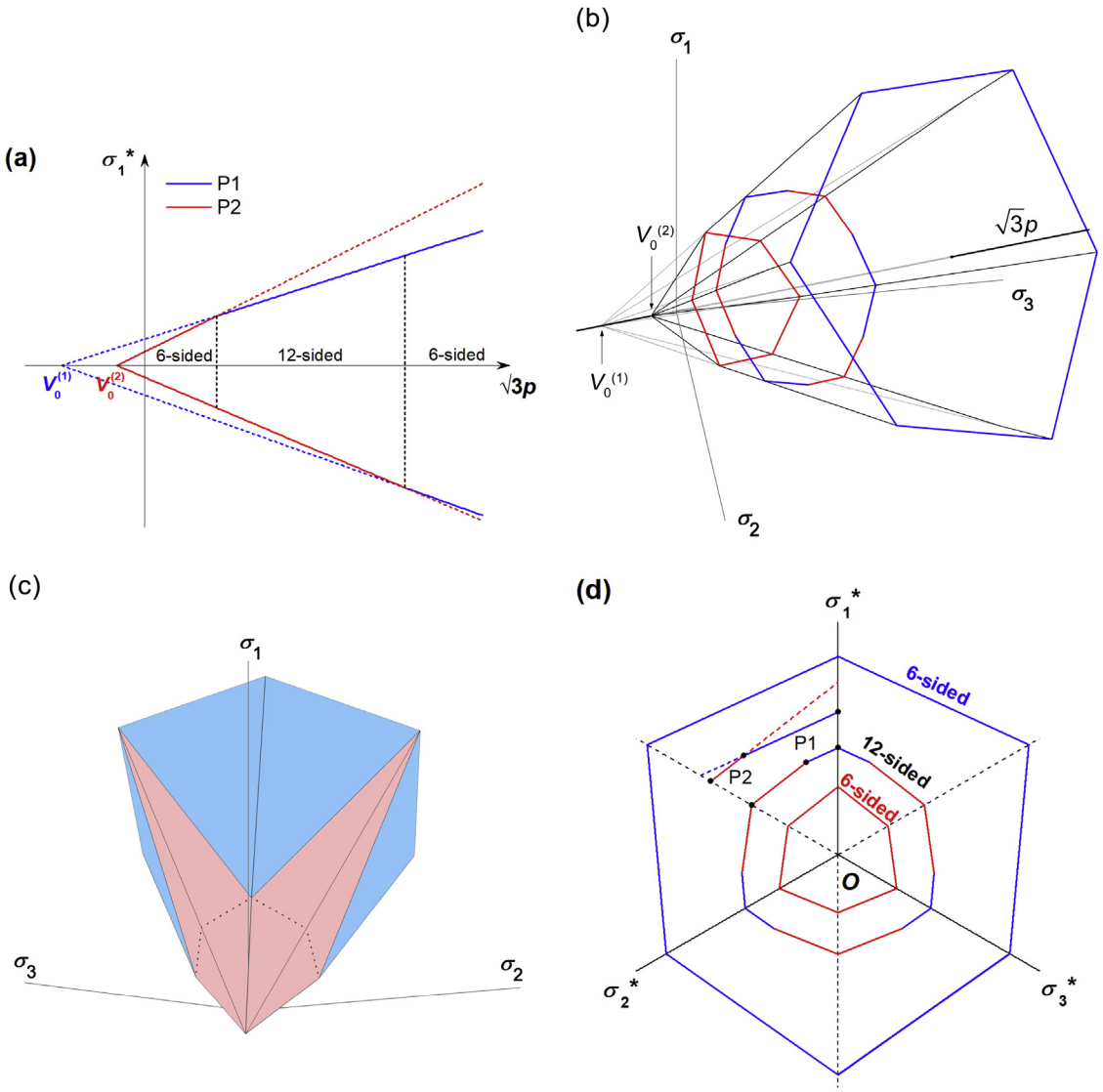

Fig. 12. Six-parameter PMC featuring the evolution of the 6-sided to 12-sided to 6-sided pyramidal failure surface in the (a) $\sqrt{3}p$, σ_1^* plane; (b) principal stress space, transparent view; (c) principal stress space, opaque view; (d) π-plane.

reports the material parameters for the six rocks along with the goodness of fit, represented by $R^2 \geq 0.96$. For the six rocks examined, $\phi_e \geq \phi_c$ and this is a consequence of the intermediate stress effect.

5.2. PMC with six parameters

To approximate, in a piecewise linear manner, a nonlinear failure surface, two planes can be fitted resulting in six material parameters. Due to strength isotropy, there are six ways to orient these two planes and the failure surface is formed by two irregular 6-sided pyramids. Depending on the values of the six parameters, four possible representations appear: (i) 12-sided; (ii) 6-sided to 12-sided to 6-sided, represented in Fig. 12; (iii) 6-sided to 12-sided, represented in Fig. 13; and (iv) 6-sided to 6-sided, represented in Fig. 14. The 12-sided pyramidal failure surface is a special case and requires $V_0^{(1)} = V_0^{(2)}$, which must be forced, and the 12-sided pyramidal failure surface was discussed by Meyer and Labuz (2013). For conditions (ii), (iii), and (iv), Figs. 12–14 are sketches of the PMC failure surfaces with six parameters in the (a) $\sqrt{3}p$, σ_1^* plane, which is the cross-section of the failure surface in principal stress space and directly related to the p, q plane; (b) principal stress space with transparent failure surfaces; (c) principal stress space with opaque failure surfaces; and (d) π-plane with $V_0^{(1)} \geq V_0^{(2)}$ for the failure surface to be convex in the p, q plane.

The rule for constructing the failure surface is that the stress state at failure always follows the line that is closer to the p-axis in the p, q plane – the smaller q – and the failure surface is represented by solid lines in the $\sqrt{3}p$, σ_1^* plane of Figs. 12a, 13a and 14a. Consequently, the two planes of the six-parameter PMC model are represented as lines, blue for P1 and red for P2. Because the failure lines for axisymmetric compression and extension can intersect at different values of p, a 12-sided failure surface forms within a certain range of mean stress, with changing shape on the π-plane; the failure surface is 6-sided outside this region. Fig. 14a shows a special situation in that the intersection points for compression and extension are at the same p, which results in a failure surface that is always a 6-sided pyramid.

Fig. 12 illustrates the 6-sided to 12-sided and back to 6-sided pyramidal failure surface, where $\phi_c^{(1)} < \phi_c^{(2)}$ and $\phi_e^{(1)} < \phi_e^{(2)}$ are required in this situation. At low mean stress, P2 controls failure, as identified by the solid red lines and the failure surface is 6-sided; this is shown in principal stress space (Fig. 12b and c) and in the π-plane (Fig. 12d). As mean stress increases, P2 intersects P1 on the compression side, and the 6-sided failure surface switches to 12-sided, which is illustrated in Fig. 12b, c, and 12d. On the π-plane, the shape change with mean stress is clearly visible and this phenomenon has been

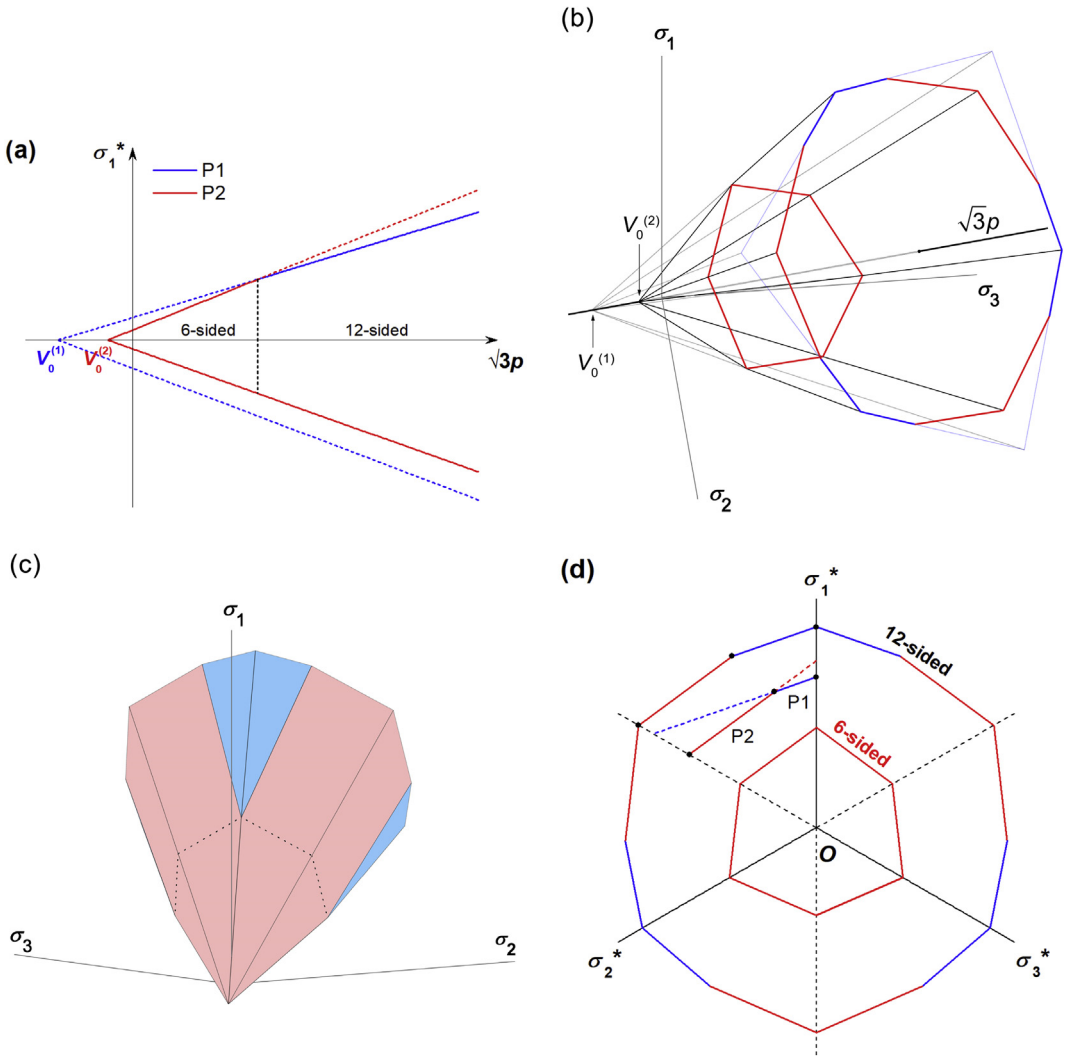

Fig. 13. Six-parameter PMC featuring the evolution of 6-sided to 12-sided pyramidal failure surface in the (a) $\sqrt{3}p$, σ_1^* plane; (b) principal stress space, transparent view; (c) principal stress space, opaque view; (d) π-plane.

experimentally observed by Descamps et al. (2012), Ingraham et al. (2013), and Makhnenko et al. (2015), among others. With increasing mean stress, P2 intersects P1 on the extension side and the failure surface switches back to a 6-sided pyramid controlled by P1. Note that type (ii) captures the decreasing slope of the failure surface in the *p, q* plane for all stress states between compression and extension, and thus of the four types, (ii) is the expected to be representative of most rock.

Fig. 13 shows the 6-sided to 12-sided pyramidal failure surface with $\phi_c^{(1)} < \phi_c^{(2)}$ and $\phi_e^{(1)} \geq \phi_e^{(2)}$. Because the failure lines for extension do not intersect in the $\sqrt{3}p$, σ_1^* plane on the $-\sigma_1^*$ side (Fig. 13a), the pyramidal failure surface stays 12-sided as mean stress increases. It is also possible that the pyramidal surface is 6-sided to 12-sided if the failure lines for compression do not intersect, $\phi_c^{(1)} \geq \phi_c^{(2)}$ and $\phi_e^{(1)} < \phi_e^{(2)}$. Type (iii) does not feature the decreasing slope of the failure surface in the *p, q* plane for either compression or extension and this is probably due to insufficient experimental data. For the 12-sided failure surface in the π-plane, the shape changes with changing mean stress (Fig. 13d).

Fig. 14 is a special case of a 6-sided to 6-sided pyramidal failure surface, where the lines for P2 and P1 intersect at the same mean stress $p_c = p_e$ on the compression and extension regions (Fig. 14a). The failure surface remains 6-sided with two different irregular hexagonal pyramids (Fig. 14b and c). Based on Eqs. (23), (35) and (36), the points p_c for compression ($\theta = 0^\circ$) and p_e for extension ($\theta = 60^\circ$) are

$$p_c = \frac{3(V_0^{(1)} \sin\phi_c^{(1)} - V_0^{(2)} \sin\phi_c^{(2)}) - (V_0^{(1)} - V_0^{(2)})\sin\phi_c^{(1)} \sin\phi_c^{(2)}}{3(\sin\phi_c^{(2)} - \sin\phi_c^{(1)})} \tag{37}$$

$$p_e = \frac{3(V_0^{(1)} \sin\phi_e^{(1)} - V_0^{(2)} \sin\phi_e^{(2)}) + (V_0^{(1)} - V_0^{(2)})\sin\phi_e^{(1)} \sin\phi_e^{(2)}}{3(\sin\phi_e^{(2)} - \sin\phi_e^{(1)})} \tag{38}$$

and $p_c = p_e$ reduces to $F(\phi_c^{(1)}, \phi_e^{(1)}, \phi_c^{(2)}, \phi_e^{(2)})V_0^{(1)} = G(\phi_c^{(1)}, \phi_e^{(1)}, \phi_c^{(2)}, \phi_e^{(2)})V_0^{(2)}$. It can be shown that $F = G$, and because $V_0^{(1)} > V_0^{(2)}$ is required, the only possible solution is $F = G = 0$. This condition is met when $r_c^{(1)}/r_e^{(1)} = r_c^{(2)}/r_e^{(2)}$, which means that the failure surfaces in the π-plane are parallel (Fig. 14d). However, the slopes of the failure lines in the *p, q* plane are different, and thus for the same Δp the increase in Δq is different (Fig. 14d).

In summary, PMC with six parameters is capable of capturing the shape evolution of the failure surface, in the *p, q* and π-planes, based strictly on the experimental data. The requirements of the six parameters for different PMC surfaces are summarized in Table 2. Note that it is conceptually possible to develop PMC with more than two planes.

The proposed fitting method was applied to determine the six parameters, three for P1 and three for P2 independently, for six selected rocks with sufficient strength data to warrant two-plane fitting; the values are displayed in Table 3. Rather than using a 3D representation in principal stress space, it is convenient to plot the multiaxial data in the σ_I, σ_{II} plane grouped by specific values of σ_{III}. The fitted PMC failure

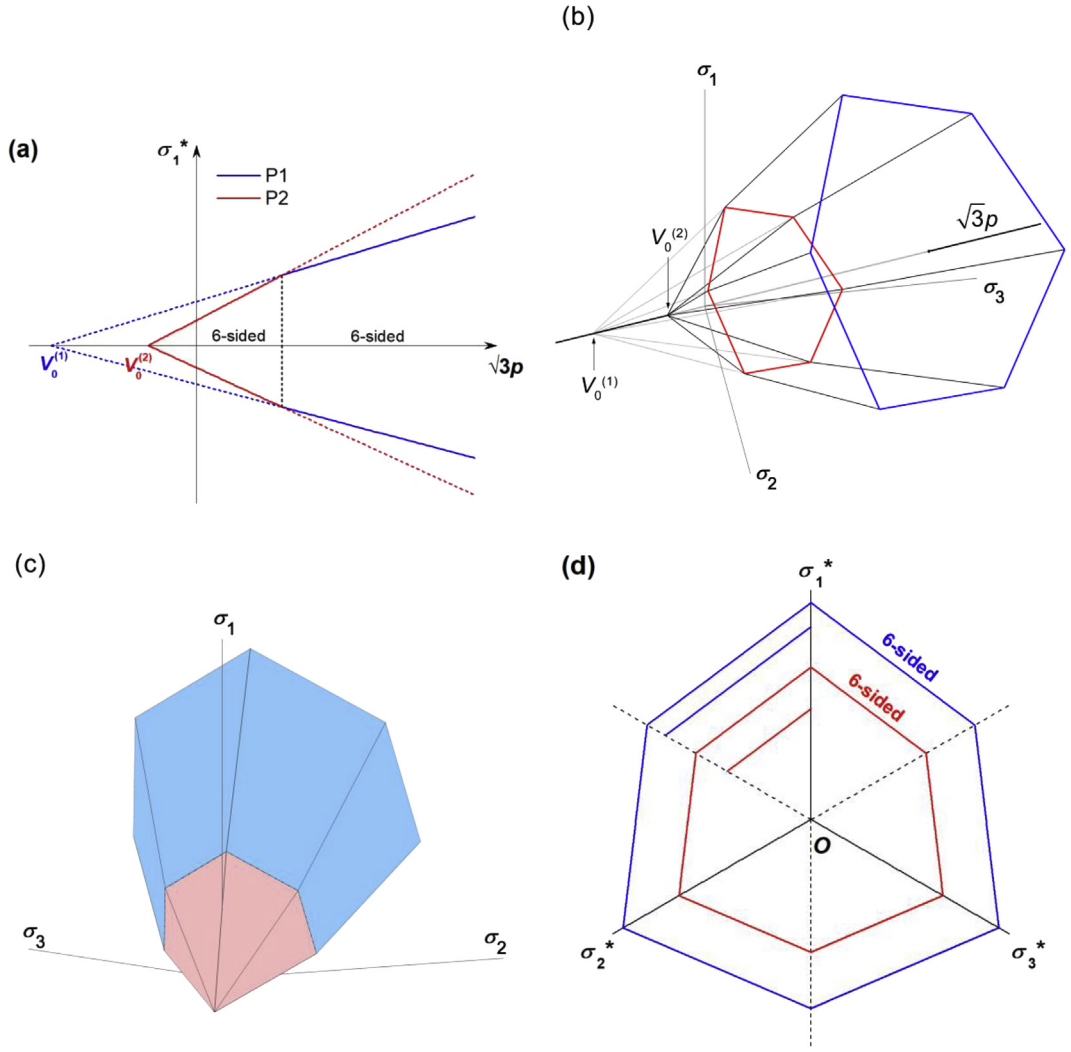

Fig. 14. Six-parameter PMC featuring the evolution of the 6-sided to 6-sided pyramidal failure surface in the (a) $\sqrt{3}p$, σ_1^* plane; (b) principal stress space, transparent view; (c) principal stress space, opaque view; (d) π-plane.

Table 2
Four types of PMC failure surfaces with six parameters (two planes).

Type of PMC failure surface	Requirements of parameters
(i), 12-sided	$V_0^{(1)} = V_0^{(2)}$
(ii), 6-12-6 sided	$\phi_c^{(1)} < \phi_c^{(2)}$, $\phi_e^{(1)} < \phi_e^{(2)}$, $p_c \neq p_e$
(iii), 6–12 sided	$\phi_c^{(1)} < \phi_c^{(2)}$, $\phi_e^{(1)} \geq \phi_e^{(2)}$; or $\phi_c^{(1)} \geq \phi_c^{(2)}$, $\phi_e^{(1)} < \phi_e^{(2)}$
(iv), 6-6 sided	$\phi_c^{(1)} < \phi_c^{(2)}$, $\phi_e^{(1)} < \phi_e^{(2)}$, $p_c = p_e$

Note: $V_0^{(1)} > V_0^{(2)}$ and $0^\circ \leq \phi_{c,e}^{(i)} < 90^\circ$.

surface intersects the σ_I, σ_{II} plane as a branch of failure lines at various values of σ_{III}. Two rock types, Mizuho trachyte (Mogi, 1971) and Taiwan siltstone (Haimson and Rudnicki, 2010), are considered. Fig. 15 shows the comparison of the six-parameter PMC failure surfaces and the experimental data for the two rocks. For Fig. 15a, a type (ii) failure surface as shown by the inset figure, the axisymmetric compression lines have the slope of $[1 + (1/N_c^{(i)})]$; the red line is associated with P2 and $\phi_c^{(2)}$ while the blue line with P1 and $\phi_c^{(1)}$. Only one axisymmetric compression line appears in Fig. 15b because of the type (iii) failure surface as shown by the inset figure. The failure lines, red for P2 and blue for P1, at each constant σ_{III} in the σ_I, σ_{II} plane are in reasonable agreement with the experimental data ($R^2 \geq 0.96$). The piecewise linear segments at constant σ_{III}, each with slope $[1 - (N_e^{(i)}/N_c^{(i)})]$

Table 3
Values of the six PMC parameters and types of failure surface for selected rock; see Tables A7–A12 for data.

Rock	Reference	Type of failure surface	$\phi_c^{(1)}$ (°)	$\phi_e^{(1)}$ (°)	$V_0^{(1)}$ (MPa)	R_1^2	$\phi_c^{(2)}$ (°)	$\phi_e^{(2)}$ (°)	$V_0^{(2)}$ (MPa)	R_2^2
Mizuho trachyte	Mogi (1971)	(ii)	28.1	28.6	126.4	0.98	30.7	40.5	73.1	0.96
Shirahama sandstone	Takahashi and Koide (1989)	(iii)	37.4	46.4	26.0	0.98	41.2	38.9	25.2	0.99
Taiwan siltstone	Haimson and Rudnicki (2010)	(iii)	31.5	27.8	61.0	0.97	29.7	39.8	46.2	0.99
Coconino sandstone	Ma and Haimson (2016)	(ii)	36.7	34.9	58.2	0.98	39.6	45.6	30.7	0.97
Bentheim sandstone	Ma and Haimson (2016)	(ii)	34.7	32.3	32.7	0.98	36.6	47.5	14.5	0.98
Dunnville sandstone	Zeng et al. (2018)	(ii)	14.3	13.0	84.7	0.99	33.9	34.5	11.9	0.99

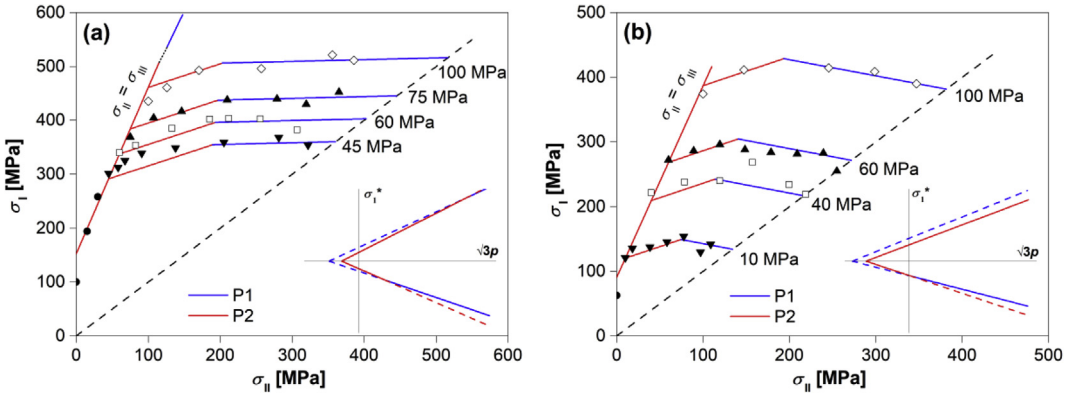

Fig. 15. Six-parameter PMC and data in the σ_I, σ_{II} plane from strength tests on (a) Mizuho trachyte (Mogi, 1971); (b) Taiwan siltstone (Haimson and Rudnicki, 2010). The insets feature the PMC failure surfaces in the $\sqrt{3}p$, σ_1^* planes.

where i = P1 and P2, exhibit a convexity of the failure surface.

5.3. Simplified PMC with four parameters

Because the application of the six-parameter PMC demands experimental data that involves multiaxial testing, a simplified version of PMC with four material parameters is proposed by considering only triaxial compression data and assuming two piecewise linear MC failure envelopes, which means that $\phi_c^{(1)} = \phi_e^{(1)} = \phi^{(1)}$ for P1 and $\phi_c^{(2)} = \phi_e^{(2)} = \phi^{(2)}$ for P2. The result is similar to a PMC failure surface of type (ii), a 6-sided to 12-sided to 6-sided pyramid. The two 6-sided pyramids are MC failure surfaces at two different friction angles $\phi^{(1)} < \phi^{(2)}$ and the 12-sided pyramid provides a transition. As an example, consider only the triaxial compression data for Dunnville sandstone in the p, q plane (Fig. 16), where two piecewise linear segments P1 and P2 fit the data with $R^2 \geq 0.98$. Table 4 shows the six-parameter PMC and the simplified PMC values, which match reasonably well. Thus, the simplified PMC using only triaxial compression data can provide an approximation to a nonlinear failure surface.

The intersection points in the p, q plane of the two failure lines for axisymmetric compression and extension represent stress states meeting the failure conditions of both P1 and P2, and in between p_c and p_e the failure surface is 12-sided. Instead of two points in the p, q plane, the stress states are represented by one circle in a Mohr diagram (Fig. 17), which is simultaneously tangent to the failure envelopes associated with P1 and P2, and σ_{II} varies from σ_I to σ_{III}. Fig. 17 shows the piecewise linear segments of the failure envelope connected by the black solid arc of the Mohr circle between the two points of tangency. Also included in Fig. 17 is the tension cut-off as it appears in the Mohr plane; the circle forming the tension cut-off is associated with the stress state $\sigma_I = [C_0 - T(N + 1)/N]$, $\sigma_{III} = -T$. If the compression and extension friction angles differ, which is not the case for the simplified PMC, then the piecewise linear failure envelope in the Mohr plane must represent compression and extension situations separately.

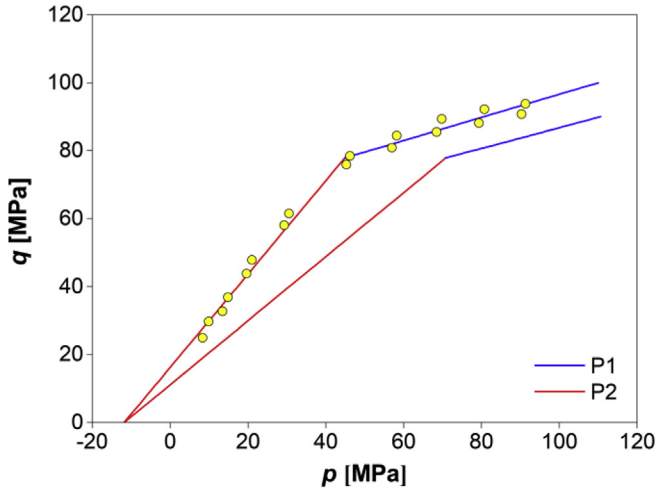

Fig. 16. Simplified PMC failure surfaces, compression and extension, in the p, q plane and data from axisymmetric compression tests on Dunnville sandstone (Zeng et al. 2018).

5.4. Equivalent MC friction angle

Considering the MC failure criterion, Eq. (12), an effective (van Eekelen, 1980) or equivalent MC friction angle ϕ_θ can be defined by

$$\sigma_I = \frac{1 + \sin\phi_\theta}{1 - \sin\phi_\theta}\sigma_{III} + \frac{2V_0 \sin\phi_\theta}{1 - \sin\phi_\theta} \tag{39}$$

Given the PMC failure surface and a known stress state (σ_I, σ_{II}, σ_{III}), the MC failure surface through that stress state is associated with the equivalent friction angle ϕ_θ. Substituting Eq. (24) into Eq. (39) and simplifying provides an expression of MC in terms of p, q, θ:

$$q = \frac{3\sin\phi_\theta V_0}{\left[\cos\theta(1 - \sin\phi_\theta) + \sin\left(\frac{\pi}{6} + \theta\right)(1 + \sin\phi_\theta)\right]}\left(\frac{p}{V_0} + 1\right) \tag{40}$$

Equating q from PMC, Eq. (23), with q from Eq. (40) and inserting Eq. (29) gives

$$\frac{3\sin\phi_\theta V_0}{\cos\theta(1 - \sin\phi_\theta) + \sin\left(\frac{\pi}{6} + \theta\right)(1 + \sin\phi_\theta)} = \frac{b_c}{\cos\theta - k\sin\theta} \tag{41}$$

The equivalent MC friction angle ϕ_θ can be expressed by ϕ_c and ϕ_e by substituting Eqs. (35) and (36) into Eq. (41):

$$\sin\phi_\theta = \frac{(3\sqrt{3}\cos\theta + 3\sin\theta)\sin\phi_c}{(\sqrt{3}\cos\theta - 3\sin\theta)\sin\phi_c + (3 - \sin\phi_c)\left(\sqrt{3}\cos\theta - \sin\theta + \frac{2\sin\phi_c(3 + \sin\phi_e)\sin\theta}{\sin\phi_e(3 - \sin\phi_c)}\right)} \tag{42}$$

Eq. (42) offers a systematic approach to determine an equivalent MC friction angle for a particular Lode angle θ, Eq. (10), which depends on the three principal stresses. For example, for PMC with three parameters, if $\phi_c = 30^\circ$ and $\phi_e = 40^\circ$ and the load direction is pure shear ($\theta = 30^\circ$), then the equivalent MC friction angle $\phi_\theta = 34.2^\circ$. If θ is known for the plane strain condition, then the corresponding plane strain friction angle can be determined. For PMC with six parameters, the calculation must consider the mean stress p and the Lode angle θ to determine which parameters, from P1 or P2, should be used in calculating the equivalent friction angle ϕ_θ because of the changing shape on the π-plane.

Table 4
PMC with four and six parameters for Dunnville sandstone.

PMC	$\phi_c^{(1)}$ (°)	$\phi_e^{(1)}$ (°)	$V_0^{(1)}$ (MPa)	R_1^2	$\phi_c^{(2)}$ (°)	$\phi_e^{(2)}$ (°)	$V_0^{(2)}$ (MPa)	R_2^2
4 parameters	9.3	9.3	184.4	0.98	34.0	34.0	11.8	0.99
6 parameters	14.3	13.0	84.7	0.99	33.9	34.5	11.9	0.99

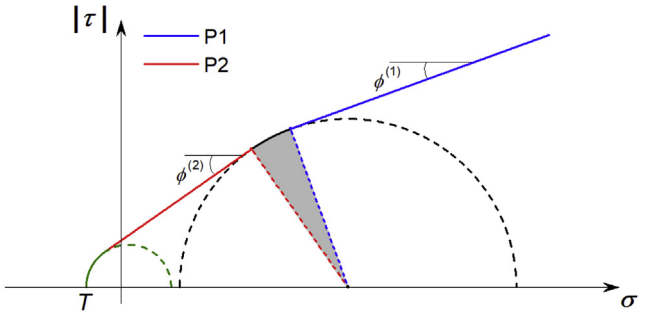

Fig. 17. Piecewise linear segments of a PMC failure envelope, including a tension cut-off, in a Mohr diagram.

6. Conclusions

"If one should succeed in finding a few rules under which many experiences could be subordinated – of course rules in which some confidence can be placed – no law of nature would have been derived, but some means found for judging the probability of new results of experience." (Mohr, O., 1901, Zur festigkeitslehre. Z. Ver. deut. Ing., p 740, from Nadai, 1950)

Failure criteria for rock are typically developed through a phenomenological approach, where the details of the material's micromechanisms are disregarded. The criterion is postulated as a function of principal stresses or other stress invariants and compared to strength tests on laboratory specimens subjected to known stress states, preferably at a minimum from both axisymmetric compression and extension tests. The best fit to the experimental data of the mathematical function (failure criterion) provides material parameters for the particular rock. Based on the results of strength tests, the selection of the failure criterion for rock should include pressure dependence (friction) that may change with mean stress.

A general linear failure criterion called Paul-Mohr-Coulomb (PMC) contains three principal stresses and provides a linear pressure-dependent strength theory capable of describing brittle failure of rock. A least-squares fitting approach was developed to determine the three PMC material parameters describing one plane: two friction angles, one for axisymmetric compression and one for axisymmetric extension, and the theoretical isotropic tensile strength V_0. Experimental results for several rock types were used to evaluate the three-parameter criterion. The fitted PMC failure surfaces show that the friction angle in extension is larger than the friction angle in compression for the rock considered, indicating an intermediate stress effect.

To approximate, in a piecewise linear manner, a nonlinear failure surface, two planes can be fitted resulting in six material parameters: four friction angles and two values of V_0. The six-parameter PMC criterion has three major features: (i) it describes the convex nature of the failure surface, including the intermediate stress effect; (ii) it characterizes the shape evolution of the failure surface in the equipressure plane (plane normal to the hydrostatic axis); and (iii) it approximates the nonlinear variation of deviatoric stress with mean stress, all by piecewise linear segments. The six-parameter PMC criterion is evaluated with multiaxial strength data on several rock types, and the fitted failure surfaces agree well with the experimental data. Thus, the general linear model of PMC is a mathematically convenient and physically attractive failure criterion to describe brittle failure of rock.

Notation

The following symbols are used in the paper:

A, B, C	material parameters
A	rectangular data matrix
b	data vector
b_c	intercept of axisymmetric compression line in p, q plane
b_e	intercept of axisymmetric extension line in p, q plane
b_θ	intercept of multiaxial line in p, q plane
C_0	uniaxial compressive strength
c	cohesion
E_{eff}	effective Young's modulus
I_1	first invariant of stress state
J_2	second invariant of deviator stress
J_3	third invariant of deviator stress
K_{eff}	effective bulk modulus
K_s	bulk modulus of solid
k	slope of PMC failure line in π-plane
m	$(\eta + 1)^{1/2}$ for Fairhurst criterion
m_b	parameter for Hoek-Brown criterion
N	MC material parameter
N_c	PMC material parameter associated with compression

Acknowledgements

This research was partially funded, with no endorsement of the approach, by the MSES/Miles Kersten Chair, China Scholarship Council, DOE grant DE-FE0002020, NSF grant CMMI-0825454, and Itasca Consulting Inc. We are indebted to Andrew Drescher for discussions on failure criteria and plasticity theory. Yves Guéguen and John Rudnicki provided valuable comments.

N_e	PMC material parameter associated with extension
n	porosity
p	mean stress or hydrostatic stress
p_c	mean stress of P1 and P2 intersection point in p, q for compression
p_e	mean stress of P1 and P2 intersection point in p, q for extension
$P1$	plane 1
$P2$	plane 2
q	deviatoric stress
q_c	deviatoric stress for triaxial compression
q_e	deviatoric stress for triaxial extension
r_c	radial distance in π-plane for triaxial compression
r_e	radial distance in π-plane for triaxial extension
r_θ	radial distance in π-plane for multiaxial testing
S_0	shear stress intercept on Mohr diagram
S_{ij}	deviator stress
T	uniaxial tensile strength
T_0	theoretical uniaxial tensile strength
V_0	theoretical isotropic tensile strength
$V_0^{(1)}$	theoretical isotropic tensile strength for P1
$V_0^{(2)}$	theoretical isotropic tensile strength for P2
$\mathbf{x}$	parameter vector
α	b_c/b_e
β	q_e/q_c in the Willam-Warnke shape function
δ_{ij}	Kronecker delta
ε_{I}, $\varepsilon_{\mathrm{II}}$, $\varepsilon_{\mathrm{III}}$	major, intermediate, minor principal strains
ε_a	axial strain
ε_v	volumetric strain
ϕ	friction angle
$\phi^{(1)}$	friction angle for P1
$\phi^{(2)}$	friction angle for P2
ϕ_c	friction angle for axisymmetric compression
$\phi_c^{(1)}$	compression friction angle for P1
$\phi_c^{(2)}$	compression friction angle for P2
ϕ_e	friction angle for axisymmetric extension
$\phi_e^{(1)}$	extension friction angle for P1
$\phi_e^{(2)}$	extension friction angle for P2
ϕ_θ	equivalent MC friction angle
η	C_0/T for Fairhurst criterion
ν_s	Poisson's ratio of solid
θ	angle from σ_1^* direction in π-plane
ρ	crack density
σ	normal stress
σ_{ij}	stress component
$\sigma_{m,\,2}$	$(\sigma_{\mathrm{I}} + \sigma_{\mathrm{III}})/2$
σ_{I}, σ_{II}, σ_{III}	major, intermediate, minor principal stresses
σ_1, σ_2, σ_3	principal stresses with no regard to magnitude
σ_1^*, σ_2^*, σ_3^*	projections of the principal stress axes in π-plane
σ_a	axial stress
τ	shear stress
τ_{oct}	octahedral shear stress

Appendix. Experimental data

Table A1
Darley Dale sandstone (Murrell, 1965).

σ_1 (MPa)	σ_2 (MPa)	σ_3 (MPa)	p (MPa)	q (MPa)	θ (°)
79.3	0	0	26.4	79.3	0
108.6	3.4	3.4	38.5	105.1	0
137.9	6.9	6.9	50.6	131.0	0
171.3	13.8	13.8	66.3	157.5	0
187.5	17.2	17.2	74.0	170.3	0
222.0	24.1	24.1	90.1	197.9	0
255.1	34.5	34.5	108.0	220.6	0

(continued on next page)

Table A1 (*continued*)

σ_1 (MPa)	σ_2 (MPa)	σ_3 (MPa)	p (MPa)	q (MPa)	θ (°)
326.1	51.7	51.7	143.2	274.4	0
401.3	68.9	68.9	179.7	332.3	0
433.7	89.6	89.6	204.3	344.0	0
502.3	110.3	110.3	241.0	392.0	0
548.8	124.1	124.1	265.7	424.7	0
586.1	137.9	137.9	287.3	448.2	0
146.2	146.2	5.3	99.2	140.9	60.0
182.7	182.7	10.9	125.4	171.8	60.0
272.3	272.3	29.7	191.5	242.6	60.0

Table A2
Yuubari shale (Takahashi and Koide, 1989).

σ_1 (MPa)	σ_2 (MPa)	σ_3 (MPa)	p (MPa)	q (MPa)	θ (°)
161.0	25.0	25.0	70.3	136.0	0
168.0	25.0	25.0	72.7	143.0	0
182.0	35.0	25.0	80.7	152.2	3.3
187.0	36.0	25.0	82.7	156.8	3.5
175.0	45.0	25.0	81.7	141.1	7.1
175.0	56.0	25.0	85.3	137.2	11.3
186.0	66.0	25.0	92.3	144.9	14.2
200.0	77.0	25.0	100.7	155.7	16.8
194.0	79.0	25.0	99.3	149.5	18.2
196.0	85.0	25.0	102.0	150.3	20.2
201.0	96.0	25.0	107.3	153.4	23.6
194.0	100.0	25.0	106.3	146.7	26.3
186.0	114.0	25.0	108.3	139.7	33.5
197.0	124.0	25.0	115.3	149.5	35.0
183.0	133.0	25.0	113.7	139.9	42.0
228.0	50.0	50.0	109.3	178.0	0
239.0	50.0	50.0	113.0	189.0	0
245.0	50.0	50.0	115.0	195.0	0
257.0	69.0	50.0	125.3	198.2	4.8
261.0	90.0	50.0	133.7	194.1	10.3
266.0	100.0	50.0	138.7	195.8	12.8
260.0	110.0	50.0	140.0	187.3	16.1
260.0	122.0	50.0	144.0	184.8	19.7
266.0	148.0	50.0	154.7	187.3	26.9
256.0	159.0	50.0	155.0	178.5	31.9

Table A3
Red Wildmoor sandstone (Papamichos et al., 2000).

σ_1 (MPa)	σ_2 (MPa)	σ_3 (MPa)	p (MPa)	q (MPa)	θ (°)
17.0	7.8	0.4	8.4	14.4	26.4
33.4	12.3	3.5	16.4	26.6	16.6
56.0	22.5	10.0	29.5	41.2	15.2
15.1	0.4	0.4	5.3	14.7	0
21.3	1.4	1.4	8.0	19.9	0
30.0	3.5	3.5	12.3	26.5	0
41.7	6.9	6.9	18.5	34.8	0
49.8	10.3	10.3	23.5	39.5	0
60.0	60.0	8.1	42.7	51.9	60.0
52.5	52.5	5.9	37.0	46.6	60.0
48.0	48.0	4.4	33.5	43.6	60.0
45.0	45.0	3.3	31.1	41.7	60.0

Table A4
Berea sandstone (Bobich, 2005).

σ_1 (MPa)	σ_2 (MPa)	σ_3 (MPa)	p (MPa)	q (MPa)	θ (°)
79.0	0	0	26.3	79.0	0
86.7	2.0	2.0	30.2	84.7	0
208.6	20.0	20.0	82.9	188.6	0
256.2	40.0	40.0	112.1	216.2	0
305.6	50.0	50.0	135.2	255.6	0
427.5	100.0	100.0	209.2	327.5	0
20.0	20.0	−7.7	10.8	27.7	60.0
30.0	30.0	−7.7	17.4	37.7	60.0
40.0	40.0	−6.9	24.4	46.9	60.0
50.0	50.0	−7.8	30.7	57.8	60.0
60.0	60.0	−6.2	37.9	66.2	60.0
70.0	70.0	−5.4	44.9	75.4	60.0
80.0	80.0	−2.1	52.6	82.1	60.0
90.0	90.0	−2.1	59.3	92.1	60.0
100.0	100.0	0.3	66.8	99.7	60.0
110.0	110.0	0.3	73.4	109.7	60.0
120.0	120.0	2.7	80.9	117.3	60.0
130.0	130.0	1.9	87.3	128.1	60.0
140.0	140.0	5.2	95.1	134.8	60.0
150.0	150.0	6.8	102.3	143.2	60.0
160.0	160.0	9.3	109.8	150.7	60.0

Table A5
Apulian calcarenite (Meyer and Labuz, 2013).

σ_1 (MPa)	σ_2 (MPa)	σ_3 (MPa)	p (MPa)	q (MPa)	θ (°)
23.9	5.0	5.0	11.3	18.9	0
19.3	2.5	2.5	8.1	16.8	0
17.4	1.25	1.25	6.6	16.2	0
19.0	1.25	1.25	7.2	17.8	0
22.3	2.5	2.5	9.1	19.8	0
25.5	5.0	5.0	11.8	20.5	0
20.5	2.1	2.1	8.2	18.4	0
18.0	0.9	0.9	6.6	17.1	0
24.5	3.9	3.9	10.8	20.6	0
18.0	0.7	0.7	6.5	17.3	0
19.5	19.5	1.2	13.4	18.3	60.0
18.0	18.0	0.3	12.1	17.7	60.0
23.7	23.7	2.6	16.7	21.1	60.0
24.0	24.0	2.6	16.9	21.4	60.0
20.0	20.0	1.2	13.7	18.8	60.0
16.8	16.8	0.1	11.2	16.7	60.0
18.0	18.0	1.1	12.4	16.9	60.0
21.8	21.8	2.7	15.4	19.1	60.0
18.0	18.0	0.4	12.1	17.6	60.0
21.8	21.8	2.5	15.4	19.3	60.0

Table A6
Indiana limestone (Makhnenko and Labuz, 2014).

σ_1 (MPa)	σ_2 (MPa)	σ_3 (MPa)	p (MPa)	q (MPa)	θ (°)
69.7	5.0	5.0	26.6	64.7	0
82.2	10.0	10.0	34.1	72.2	0
103.1	15.0	15.0	44.4	88.1	0
100.8	20.0	20.0	46.9	80.8	0
114.8	25.0	25.0	54.9	89.8	0
133.2	30.0	30.0	64.4	103.2	0
50.0	50.0	0.7	33.6	49.3	60.0
58.0	58.0	2.6	39.5	55.4	60.0
60.0	60.0	1.7	40.6	58.3	60.0
62.0	62.0	2.1	42.0	59.9	60.0
45.4	8.4	0	17.9	41.8	10.0
61.2	16.8	5.0	27.7	51.3	11.5
101.0	26.4	10.0	45.8	84.0	9.7

Table A7
Mizuho trachyte (Mogi, 1971).

σ_1 (MPa)	σ_2 (MPa)	σ_3 (MPa)	p (MPa)	q (MPa)	θ (°)
100.0	0	0	33.3	100.0	0
194.3	15.0	15.0	74.8	179.3	0
258.3	30.0	30.0	106.1	228.3	0
301.3	45.0	45.0	130.4	256.3	0
312.7	58.1	45.0	138.6	261.4	2.5
325.5	67.7	45.0	146.1	269.9	4.2
338.9	90.9	45.0	158.3	273.9	8.4
349.1	137.8	45.0	177.3	267.0	17.3
359.1	205.4	45.0	203.2	272.0	30.7
368.2	281.7	45.0	231.6	289.8	45.0
354.0	322.1	45.0	240.4	294.4	54.6
340.0	60.0	60.0	153.3	280.0	0
353.4	82.7	60.0	165.4	282.8	4.0
385.2	132.9	60.0	192.7	295.6	12.3
401.8	185.6	60.0	215.8	299.5	21.3
403.7	212.1	60.0	225.3	298.3	26.2
402.4	255.8	60.0	239.4	297.5	34.7
382.3	307.0	60.0	249.8	292.0	47.1
368.7	75.0	75.0	172.9	293.7	0
404.3	107.5	75.0	195.6	314.3	5.1
416.7	146.5	75.0	212.7	312.2	11.4
437.6	210.0	75.0	240.9	317.4	21.6
439.6	278.9	75.0	264.5	316.5	33.9
429.7	319.5	75.0	274.7	314.4	42.3
452.2	365.2	75.0	297.5	342.1	47.3
435.3	100.0	100.0	211.8	335.3	0
461.0	126.0	100.0	229.0	348.7	3.7
492.8	170.4	100.0	254.4	362.8	9.7
496.0	257.3	100.0	284.4	345.4	23.2
521.4	356.0	100.0	325.8	367.8	37.1
511.7	385.9	100.0	332.5	365.4	42.7

Table A8
Shirahama sandstone (Takahashi and Koide, 1989).

σ_1 (MPa)	σ_2 (MPa)	σ_3 (MPa)	p (MPa)	q (MPa)	θ (°)
94.0	9.0	5.0	36.0	87.1	2.3
97.0	15.0	5.0	39.0	87.4	5.7
109.0	44.0	5.0	52.7	91.0	21.8
94.0	65.0	5.0	54.7	78.6	41.4
109.0	12.0	8.0	43.0	99.1	2.0
129.0	27.0	8.0	54.7	112.7	8.4
132.0	41.0	8.0	60.3	111.2	14.9
135.0	50.0	8.0	64.3	112.1	18.9
127.0	79.0	8.0	71.3	103.7	36.4
147.0	15.0	15.0	59.0	132.0	0
157.0	29.0	15.0	67.0	135.5	5.1
165.0	62.0	15.0	80.7	132.9	17.8
162.0	82.0	15.0	86.3	127.5	27.1
159.0	88.0	15.0	87.3	124.7	30.5
168.0	97.0	15.0	93.3	132.6	32.4
178.0	20.0	20.0	72.7	158.0	0
173.0	41.0	20.0	78.0	143.7	7.3
185.0	50.0	20.0	85.0	152.2	9.8
177.0	57.0	20.0	84.7	142.2	13.0
197.0	68.0	20.0	95.0	158.5	15.2
194.0	82.0	20.0	98.7	152.7	20.6
193.0	97.0	20.0	103.3	150.1	26.4
185.0	100.0	20.0	101.7	142.9	29.0
197.0	30.0	30.0	85.7	167.0	0
218.0	47.0	30.0	98.3	180.1	4.7
224.0	69.0	30.0	107.7	177.7	11.0
232.0	88.0	30.0	116.7	180.1	16.2
229.0	109.0	30.0	122.7	173.6	23.2
241.0	129.0	30.0	133.3	182.8	28.0
227.0	150.0	30.0	135.7	172.0	37.2
215.0	171.0	30.0	138.7	167.4	46.8
244.0	60.0	40.0	114.7	194.8	5.1
252.0	70.0	40.0	120.7	198.7	7.5
253.0	79.0	40.0	124.0	196.4	9.9
274.0	99.0	40.0	137.7	210.8	14.0
265.0	118.0	40.0	141.0	197.9	20.0
279.0	138.0	40.0	152.3	208.1	24.1
274.0	159.0	40.0	157.7	202.7	30.6

Table A9
Taiwan siltstone (Haimson and Rudnicki, 2010).

σ_1 (MPa)	σ_2 (MPa)	σ_3 (MPa)	p (MPa)	q (MPa)	θ (°)
62.8	0	0	20.9	62.8	0
121.1	10.0	10.0	47.0	111.1	0
135.4	18.1	10.0	54.5	121.6	3.3
137.6	38.6	10.0	62.1	115.9	12.3
145.2	58.1	10.0	71.1	118.7	20.5
154.0	77.5	10.0	80.5	124.8	27.9
129.7	97.0	10.0	78.9	107.2	44.7
141.8	108.9	10.0	86.9	118.8	46.1
221.3	40.0	40.0	100.4	181.3	0
237.7	78.4	40.0	118.7	181.5	10.6
239.8	119.5	40.0	133.1	174.2	23.3
268.3	157.3	40.0	155.2	197.7	30.9

(*continued on next page*)

Table A9 (*continued*)

σ_1 (MPa)	σ_2 (MPa)	σ_3 (MPa)	p (MPa)	q (MPa)	θ (°)
234.0	199.5	40.0	157.8	179.3	50.4
218.6	218.6	40.0	159.0	178.6	60.0
271.9	60.0	60.0	130.6	211.9	0
286.1	89.1	60.0	145.1	213.0	6.8
295.9	119.4	60.0	158.4	212.6	14.0
288.1	148.6	60.0	165.6	199.2	22.6
283.6	178.8	60.0	174.2	193.8	32.1
281.4	209.1	60.0	183.5	195.5	41.3
282.4	239.4	60.0	193.9	204.3	49.5
254.8	254.8	60.0	189.9	194.8	60.0
374.2	100.0	100.0	191.4	274.2	0
411.5	147.2	100.0	219.6	290.8	8.1
414.5	245.6	100.0	253.4	272.6	27.5
408.9	298.6	100.0	269.1	271.1	39.4
390.0	347.3	100.0	279.1	271.2	52.2

Table A10
Coconino sandstone (Ma and Haimson, 2016).

σ_1 (MPa)	σ_2 (MPa)	σ_3 (MPa)	p (MPa)	q (MPa)	θ (°)
56.1	0	0	18.7	56.1	0
59.5	35.0	0	31.5	51.8	35.8
76.8	76.8	0	51.2	76.8	60.0
161.8	10.0	10.0	60.6	151.8	0
187.6	90.0	10.0	95.9	154.1	26.7
170.9	170.9	10.0	117.3	160.9	60.0
235.2	20.0	20.0	91.7	215.2	0
244.2	40.0	20.0	101.4	214.9	4.6
252.4	60.0	20.0	110.8	215.2	9.3
247.3	90.0	20.0	119.1	201.6	17.5
258.8	100.0	20.0	126.3	210.5	19.2
244.6	110.0	20.0	124.9	195.8	23.5
251.9	130.0	20.0	134.0	200.9	28.3
260.1	150.0	20.0	143.4	208.2	32.7
249.0	180.0	20.0	149.7	203.5	42.9
237.2	200.0	20.0	152.4	201.2	50.8
215.0	214.4	20.0	149.8	194.7	59.8
225.9	225.9	20.0	157.3	205.9	60.0
347.2	50.0	50.0	149.1	297.2	0
360.7	90.0	50.0	166.9	292.8	6.8
368.3	125.0	50.0	181.1	288.2	13.0
372.8	160.0	50.0	194.3	284.2	19.6
354.2	200.0	50.0	201.4	263.5	29.5
377.0	205.0	50.0	210.7	283.3	28.3
365.0	240.0	50.0	218.3	274.7	36.8
352.2	275.0	50.0	225.7	271.9	45.8
364.8	310.0	50.0	241.6	291.3	50.6
341.3	341.3	50.0	244.2	291.3	60.0
427.7	80.0	80.0	195.9	347.7	0
452.0	120.0	80.0	217.3	353.7	5.6
482.2	165.0	80.0	242.4	367.2	11.6
471.5	210.0	80.0	253.8	345.4	19.0
439.1	245.0	80.0	254.7	311.3	27.3
459.4	250.0	80.0	263.1	329.2	26.6
471.0	335.0	80.0	295.3	343.8	40.0
429.9	429.9	80.0	313.3	349.9	60.0

Table A11
Bentheim sandstone (Ma and Haimson, 2016).

σ_1 (MPa)	σ_2 (MPa)	σ_3 (MPa)	p (MPa)	q (MPa)	θ (°)
30.0	0	0	10.0	30.0	0
29.7	20.0	0	16.6	26.2	41.3
39.3	39.3	0	26.2	39.3	60.0
85.1	8.0	8.0	33.7	77.1	0
109.2	50.0	8.0	55.7	88.1	24.4
84.5	84.5	8.0	59.0	76.5	60.0
122.4	15.0	15.0	50.8	107.4	0
147.0	70.0	15.0	77.3	114.8	24.5
119.5	119.5	15.0	84.7	104.5	60.0
187.6	30.0	30.0	82.5	157.6	0
195.7	80.0	30.0	101.9	147.2	17.1
194.1	130.0	30.0	118.0	143.2	37.2
181.6	181.6	30.0	131.1	151.6	60.0
251.6	60.0	60.0	123.9	191.6	0
294.8	120.0	60.0	158.3	211.3	14.2
270.1	170.0	60.0	166.7	182.0	31.6
281.5	220.0	60.0	187.2	198.0	44.4
274.8	274.8	60.0	203.2	214.8	60.0

Table A12
Dunnville sandstone (Zeng et al., 2018).

σ_1 (MPa)	σ_2 (MPa)	σ_3 (MPa)	p (MPa)	q (MPa)	θ (°)
29.7	0	0	9.9	29.7	0
24.9	0	0	8.3	24.9	0
39.4	2.5	2.5	14.8	36.9	0
35.2	2.5	2.5	13.4	32.7	0
52.9	5.0	5.0	21.0	47.9	0
48.8	5.0	5.0	19.6	43.8	0
71.5	10.0	10.0	30.5	61.5	0
68.0	10.0	10.0	29.3	58.0	0
98.4	20.0	20.0	46.1	78.4	0
95.9	20.0	20.0	45.3	75.9	0
114.5	30.0	30.0	58.2	84.5	0
110.9	30.0	30.0	57.0	80.9	0
129.4	40.0	40.0	69.8	89.4	0
125.5	40.0	40.0	68.5	85.5	0
142.1	50.0	50.0	80.7	92.1	0
138.1	50.0	50.0	79.4	88.1	0
153.8	60.0	60.0	91.3	93.8	0
150.8	60.0	60.0	90.3	90.8	0
35.0	35.0	0.8	23.6	34.2	60.0
40.0	40.0	1.2	27.1	38.8	60.0
40.0	40.0	1.8	27.3	38.2	60.0
50.0	50.0	6.0	35.3	44.0	60.0
50.0	50.0	5.7	35.2	44.3	60.0
60.0	60.0	10.1	43.4	49.9	60.0
60.0	60.0	8.0	42.7	52.0	60.0
69.0	69.0	11.5	49.8	57.5	60.0
90.0	90.0	25.7	68.6	64.3	60.0
120.0	120.0	49.3	96.4	70.7	60.0
134.0	134.0	55.7	107.9	78.3	60.0

References

Akai, K., Mori, H., 1967. Study on the failure mechanism of a sandstone under combined compressive stresses (in Japanese). Trans. Jpn. Soc. Civ. Eng. 147, 11–24.

Al-Ajmi, A.M., Zimmerman, R.W., 2005. Relation between the Mogi and the Coulomb failure criteria. Int. J. Rock Mech. Min. Sci. 42 (3), 431–439.

Alexeev, A.D., Revva, V.N., Alyshev, N.A., Zhitlyonok, D.M., 2004. True triaxial loading apparatus and its application to coal outburst prediction. Int. J. Coal Geol. 58 (4), 245–250.

Argyris, J.H., Faust, G., Szimmat, J., Warnke, E.P., Willam, K.J., 1974. Recent developments in the finite element analysis of prestressed concrete reactor vessels. Nucl. Eng. Des. 28 (1), 42–75.

Atkinson, R.H., Ko, H.Y., 1973. A fluid cushion, multiaxial cell for testing cubical rock specimens. Int. J. Rock Mech. Min. Sci. Geomech. Abstr. 10 (4), 351–354.

Aubertin, M., Li, L., Simon, R., 2000. A multiaxial stress criterion for short- and long-term strength of isotropic rock media. Int. J. Rock Mech. Min. Sci. 37 (8), 1169–1193.

Aydin, A., Borja, R.I., Eichhubl, P., 2006. Geological and mathematical framework for failure modes in granular rock. J. Struct. Geol. 28 (1), 83–98.

Balmer, G., 1952. A general analytic solution for Mohr's envelope. Proc. Am. Soc. Test. Mater. 1260–1271.

Balmer, G.G., 1953. Physical Properties of Some Typical Foundation Rocks. US Bureau of Reclamation Concrete Lab. Rept. SP-39.

Bardet, J.P., 1990. Lode dependences for isotropic pressure-sensitive elastoplastic materials. J. Appl. Mech. 57 (3), 498–506.

Benz, T., Schwab, R., Kauther, R.A., Vermeer, P.A., 2008. A Hoek-Brown criterion with intrinsic material strength factorization. Int. J. Rock Mech. Min. Sci. 45 (2), 210–222.

Bésuelle, P., Hall, S.A., 2011. Characterization of the strain localization in a porous rock in plane strain condition using a new true-triaxial apparatus. In: Bonelli, S., Dascalu, C., Nicot, F. (Eds.), Advances in Bifurcation and Degradation in Geomaterials. Springer, Dordrecht, pp. 345–352.

Bieniawski, Z.T., Denkhaus, H.G., Vogler, U.W., 1969. Failure of fractured rock. Int. J. Rock Mech. Min. Sci. 6, 323–341.

Bigoni, D., Piccolroaz, A., 2004. Yield criteria for quasibrittle and frictional materials. Int. J. Solids Struct. 41 (11), 2855–2878.

Bobich, J.K., 2005. Experimental Analysis of the Extension to Shear Fracture Transition in Berea sandstone. M. S. thesis. Texas A&M University.

Böker, R., 1915. Die mechanik der bleibenden formänderung in kristallinisch aufgebauten körpern. Forschungsarbeiten dem Gebiete des Ingenieurwesens 175, 1–51.

Borja, R.I., 2013. Plasticity: Modeling and Computation. Springer, New York.

De Borst, R., 1987. Computation of post-bifurcation and post-failure behavior of strain-softening solids. Comput. Struct. 25 (2), 211–224.

Boswell, L.F., Chen, Z., 1987. A general failure criterion for plain concrete. Int. J. Solids Struct. 23 (5), 621–630.

Brace, W.F., 1964. Brittle fracture of rocks. In: Judd, W.R. (Ed.), State of Stress in the Earth's Crust. Elsevier, New York, pp. 111–174.

Burzynski, W., 1929. Uber die anstrengungshypothesen. Schweiz. Bauztg. 94, 259–262.

Cherry, J.T., Larson, D.B., Rapp, E.G., 1968. A unique description of the failure of a brittle material. Int. J. Rock Mech. Min. Sci. Geomech. Abstr. 5 (5), 455–463.

Davis, R.O., Selvadurai, A.P., 2002. Plasticity and Geomechanics. Cambridge University Press.

Desai, C.S., 1980. A general basis for yield, failure and potential functions in plasticity. Int. J. Numer. Anal. Methods Geomech. 4 (4), 361–375.

Desai, C.S., Salami, M.R., 1987. A constitutive model and associated testing for soft rock. Int. J. Rock Mech. Min. Sci. Geomech. Abstr. 24 (5), 299–307.

Descamps, F., da Silva, M.R., Schroeder, C., Verbrugge, J.C., Tshibangu, J.P., 2012. Limiting envelopes of a dry porous limestone under true triaxial stress states. Int. J. Rock Mech. Min. Sci. 56, 88–99.

Donath, F., 1966. A triaxial pressure apparatus for testing of consolidated or unconsolidated materials subjected to pore pressure. Test. Tech. Rock Mech. ASTM STP 402, 41–51.

Drescher, A., Vardoulakis, I., 1982. Geometric softening in triaxial tests on granular material. Géotechnique 32 (4), 291–303.

Dreyer, W., Borchert, H., 1962. Ähnlichkeitsmechanik: ein beitr. zur gesteinsphysik und gebirgsdruckforschung. Bergbuwissenschaften 9, 356–361.

Drucker, D.C., Prager, W., 1952. Soil mechanics and plastic analysis or limit design. Q. Appl. Math. 9 (2), 157–165.

Du, X., Lu, D., Gong, Q., Zhao, M., 2010. Nonlinear unified strength criterion for concrete under three-dimensional stress states. J. Eng. Mech. 136 (1), 51–59.

van Eekelen, H.A.M., 1980. Isotropic yield surfaces in three dimensions for use in soil mechanics. Int. J. Numer. Anal. Methods Geomech. 4 (1), 89–101.

Ewy, R.T., 1999. Wellbore-stability predictions by use of a modified Lade criterion. SPE Drill. Complet. 14 (2), 85–91.

Fairhurst, C., 1964. On the validity of the Brazilian test for brittle materials. Int. J. Rock Mech. Min. Sci. 1 (4), 535–546.

Feng, X.T., Zhang, X., Kong, R., Wang, G., 2016. A novel Mogi type true triaxial testing apparatus and its use to obtain complete stress–strain curves of hard rocks. Rock Mech. Rock Eng. 49 (5), 1649–1662.

Föppl, A., 1900. Abhangigkeit der bruchgefahr von der art des spannungszustandes. Mitth. Aus dem Meehnischen Tech. Laburatorium, München 27, 1–35.

Franklin, J.A., Hoek, E., 1968. Developments in triaxial testing technique. Rock Mech. Rock Eng. 2 (4), 223–228.

Griggs, D.T., 1936. Deformation of rocks under high confining pressures: I. Experiments at room temperature. J. Geol. 44 (5), 541–577.

Haimson, B., Chang, C., 2000. A new true triaxial cell for testing mechanical properties of rock, and its use to determine rock strength and deformability of Westerly granite. Int. J. Rock Mech. Min. Sci. 37 (1), 285–296.

Haimson, B., Rudnicki, J.W., 2010. The effect of the intermediate principal stress on fault formation and fault angle in siltstone. J. Struct. Geol. 32 (11), 1701–1711.

Handin, J., Hager, R.V., 1957. Experimental deformation of sedimentary rocks under confining pressure: tests at room temperature on dry samples. Bull. Am. Assoc. Petrol. Geol. 41 (1), 1–50.

Harbottle, T.B., 1906. Dictionary of Quotations (1906). 42. Bacon, Sir Francis, Novum Organum, I, 70. https://todayinsci.com/B/Bacon_Francis/BaconFrancis-Quotations.htm, Accessed date: 21 July 2017.

Haythornthwaite, R.M., 1962. Range of yield condition in ideal plasticity. Trans. Am. Soc. Civ. Eng. 127 (1), 1252–1269.

Haythornthwaite, R.M., 1985. A family of smooth yield surfaces. Mech. Res. Commun. 12 (2), 87–91.

He, M.C., Miao, J.L., Feng, J.L., 2010. Rock burst process of limestone and its acoustic emission characteristics under true-triaxial unloading conditions. Int. J. Rock Mech. Min. Sci. 47 (2), 286–298.

Heard, H.C., 1960. Transition from brittle fracture to ductile flow in Solenhofen limestone as a function of temperature, confining pressure, and interstitial fluid pressure. Geol. Soc. Am. Memoirs 79, 193–226.

Hobbs, D.W., 1970. The behavior of broken rock under triaxial compression. Int. J. Rock Mech. Min. Sci. Geomech. Abstr. 7 (2), 125–148.

Hoek, E., Brown, E.T., 1980. Empirical strength criterion for rock masses. J. Geotech. Geoenviron Eng. 106 (9), 1013–1035.

Hoek, E., Carranza-Torres, C., Corkum, B., 2002. Hoek-Brown failure criterion-2002 edition. In: Proceedings of the Fifth North American Rock Mechanics Symposium, Toronto, Canada, vol. 1. pp. 267–273.

Hojem, J.P.M., Cook, N.G.W., 1968. The design and construction of a triaxial and polyaxial cell for testing rock specimens. South Afr. Mech. Eng. 18 (2), 57–61.

Hsieh, S.S., Ting, E.C., Chen, W.F., 1982. A plastic-fracture model for concrete. Int. J. Solids Struct. 18 (3), 181–197.

Huxley, T.H. (1870). https://en.wikiquote.org/wiki/Thomas_Henry_Huxley accessed 21 July 2017.

Ingraham, M.D., Issen, K.A., Holcomb, D.J., 2013. Response of Castlegate sandstone to true triaxial states of stress. J. Geophys. Res. Solid Earth 118 (2), 536–552.

Jaeger, J.C., Cook, N.G., Zimmerman, R., 2007. Fundamentals of Rock Mechanics. John Wiley & Sons.

Jeremić, B., Sture, S., 1997. Implicit integrations in elastoplastic geotechnics. Mech. Cohes. Frict. Mater. 2 (2), 165–183.

Jiang, J., Pietruszczak, S., 1988. Convexity of yield loci for pressure sensitive materials. Comput. Geotech. 5 (1), 51–63.

Kachanov, M., 1993. Elastic solids with many cracks and related problems. Adv. Appl. Mech. 30, 259–445.

Kapang, P., Walsri, C., Sriapai, T., Fuenkajorn, K., 2013. Shear strengths of sandstone fractures under true triaxial stresses. J. Struct. Geol. 48, 57–71.

Karev, V.I., Kovalenko, Y.F., 2013. Triaxial loading system as a tool for solving geotechnical problems of oil and gas production. In: Kwaśniewski, M., Li, X., Takahashi, M. (Eds.), True Triaxial Testing of Rocks. CRC Press/Balkema, The Netherlands, pp. 301–310.

von Kármán, T., 1911. Festigkeitsversuche unter allseitigem druck. Z. Des. Vereines Dtsch. Ingenieure 55 (42), 1749–1757.

Kim, M.K., Lade, P.V., 1984. Modelling rock strength in three dimensions. Int. J. Rock Mech. Min. Sci. Geomech. Abstr. 21 (1), 21–33.

King, M.S., Chaudhry, N.A., Shakeel, A., 1995. Experimental ultrasonic velocities and permeability for sandstones with aligned cracks. Int. J. Rock Mech. Min. Sci. Geomech. Abstr. 8 (32) 376–377A.

Krenk, S., 1996. Family of invariant stress surfaces. J. Eng. Mech. 122 (3), 201–208.

Kvapil, R., Luffer, K., 1960. Beitrag zur frage der spannungsverteilung in würfelförmigen probekörpern bei triaxialer beanspruchung. Bergakad. Freiberg 12, 587–594.

Kwaśniewski, M., Li, X., Takahashi, M. (Eds.), 2013. True Triaxial Testing of Rocks. CRC Press/Balkema, The Netherlands.

Labbane, M., Saha, N.K., Ting, E.C., 1993. Yield criterion and loading function for concrete plasticity. Int. J. Solids Struct. 30 (9), 1269–1288.

Labuz, J.F., Biolzi, L., 1991. Class I vs class II stability: a demonstration of size effect. Int. J. Rock Mech. Min. Sci. Geomech. Abstr. 28 (2/3), 199–205.

Labuz, J.F., Bridell, J.M., 1993. Reducing frictional constraint in compression testing through lubrication. Int. J. Rock Mech. Min. Sci. Geomech. Abstr. 30 (4), 451–455.

Labuz, J.F., Dai, S.T., Papamichos, E., 1996. Plane-strain compression of rock-like materials. Int. J. Rock Mech. Min. Sci. Geomech. Abstr. 33 (6), 573–584.

Labuz, J.F., Makhnenko, R.Y., Dai, S.T., Biolzi, L., 2017. On yielding, failure, and softening response of rock. In: Feng, X.T. (Ed.), Rock Mechanics and Engineering: Principles. CRC Press, pp. 365–378 Chapter 12.

Lade, P.V., 1977. Elasto-plastic stress-strain theory for cohesionless soil with curved yield surfaces. Int. J. Solids Struct. 13, 1019–1035.

Lade, P.V., Duncan, J.M., 1975. Elastoplastic stress-strain theory for cohesionless soil. J. Geotech. Eng. Div. (ASCE) 101 (10), 1037–1053.

Lagioia, R., Panteghini, A., 2016. On the existence of a unique class of yield and failure criteria comprising Tresca, von Mises, Drucker–Prager, Mohr–Coulomb, Galileo–Rankine, Matsuoka–Nakai and Lade–Duncan. Proc. R. Soc. A 472 (2185). http://dx.doi.org/10.1098/rspa.2015.0713.

Lee, Y.K., Pietruszczak, S., Choi, B.H., 2012. Failure criteria for rocks based on smooth approximations to Mohr-Coulomb and Hoek-Brown failure functions. Int. J. Rock Mech. Min. Sci. 56, 146–160.

Lin, F., Bažant, Z.P., 1986. Convexity of smooth yield surface of frictional material. J. Eng. Mech. 112 (11), 1259–1262.

Ma, X., Haimson, B.C., 2016. Failure characteristics of two porous sandstones subjected to true triaxial stresses. J. Geophys. Res. Solid Earth 121 (9), 6477–6498.

Ma, X., Rudnicki, J.W., Haimson, B.C., 2017. Failure characteristics of two porous sandstones subjected to true triaxial stresses: applied through a novel loading path. J. Geophys. Res. Solid Earth 122 (4), 2525–2540.
Makhnenko, R., Labuz, J., 2014. Plane strain testing with passive restraint. Rock Mech. Rock Eng. 47 (6), 2021–2029.
Makhnenko, R., Labuz, J., 2016. Elastic and inelastic deformation of fluid-saturated rock. Philos. Trans. R. Soc. A 374, 20150422. http://dx.doi.org/10.1098/rsta.2015.0422.
Makhnenko, R.Y., Harvieux, J., Labuz, J.F., 2015. Paul-Mohr-Coulomb failure surface of rock in the brittle regime. Geophys. Res. Lett. 42 (17), 6975–6981.
Matsuoka, H., Nakai, T., 1974. Stress-deformation and strength characteristics of soil under three different principal stresses. Proc. Jpn. Soc. Civ. Eng. 232, 59–70.
Meldahl, A., 1944. A new graphical method of representing strength characteristics. Brown Bovari Rev. 31 (8), 260–267.
Menetrey, P., Willam, K.J., 1995. Triaxial failure criterion for concrete and its generalization. ACI Struct. J. 92 (3), 311–318.
Meyer, J.P., Labuz, J.F., 2013. Linear failure criteria with three principal stresses. Int. J. Rock Mech. Min. Sci. 60, 180–187.
Michelis, P., 1985. A true triaxial cell for low and high confining pressure experiments. Int. J. Rock Mech. Min. Sci. 22, 183–188.
Mills, L.L., Zimmerman, R.M., 1970. Compressive strength of plain concrete under multiaxial loading conditions. ACI J. 67 (10), 802–807.
Mogi, K., 1971. Fracture and flow of rocks under high triaxial compression. J. Geophys. Res. 76 (5), 1255–1269.
Mogi, K., 2007. Experimental Rock Mechanics. Taylor & Francis/Balkema, The Netherlands.
Mortara, G., 2008. A new yield and failure criterion for geomaterials. Géotechnique 58 (2), 125–132.
Mroz, Z., 1973. Mathematical Models of Inelastic Material Behavior. University of Waterloo, Solid Mechanics Division.
Murrell, S.A.F., 1965. The effect of triaxial stress systems on the strength of rocks at atmospheric temperatures. Geophys. J. R. Astron. Soc. 10 (3), 231–281.
Nadai, A., 1933. Theories of strength. J. Appl. Mech. 1 (3), 111–129.
Nadai, A., 1950. Theory of Flow and Fracture of Solids, vol. 1 McGraw-Hill, New York.
Niwa, Y., Kobayashi, S., 1967. Failure criterion of cement mortar under triaxial compression. Memoirs Fac. Eng. Kyoto Univ. 29, 1–15.
Niwa, Y., Kobayashi, S., Koyanagi, W., 1967. Failure criterion of light-weight aggregate concrete subjected to triaxial compression. Memoirs Fac. Eng. Kyoto Univ. 119–131.
Ord, A., Vardoulakis, I., Kajewski, R., 1991. Shear band formation in Gosford sandstone. Int. J. Rock Mech. Min. Sci. Geomech. Abstr. 28 (5), 397–409.
Ortiz, M., Popov, E.P., 1985. Accuracy and stability of integration algorithms for elastoplastic constitutive relations. Int. J. Numer. Methods Eng. 21 (9), 1561–1576.
Ottosen, N.S., 1977. A failure criterion for concrete. J. Eng. Mech. Div. 103 (EM4), 527–535.
Pan, X.D., Hudson, J.A., 1988. A simplified three dimensional Hoek-Brown yield criterion. In: ISRM International Symposium, pp. 95–103.
Panteghini, A., Lagioia, R., 2014. A fully convex reformulation of the original Matsuoka-Nakai failure criterion and its implicit numerically efficient integration algorithm. Int. J. Numer. Anal. Methods Geomech. 38 (6), 593–614.
Papamichos, E., Tronvoll, J., Vardoulakis, I., Labuz, J.F., Skjaerstein, A., Unander, T.E., Sulem, J., 2000. Constitutive testing of red Wildmoor sandstone. Mech. Cohes. Frict. Mater. 5 (1), 1–40.
Pariseau, W.G., 1994. On the significance of dimensionless failure criteria. Int. J. Rock Mech. Min. Sci. Geomech. Abstr. 31 (5), 555–560.
Paterson, M.S., 1964. Triaxial testing of materials at pressures up to 10,000 kg/cm^2. J. Ins. Eng. Aust. 36, 23–29.
Paterson, M.S., Wong, T.F., 2005. Experimental Rock Deformation – the Brittle Field. Springer-Verlag, Berlin.
Paul, B., 1961. A modification of the Coulomb-Mohr theory of fracture. J. Appl. Mech. 28 (2), 259–268.
Paul, B., 1968a. Generalized pyramidal fracture and yield criteria. Int. J. Solids Struct. 4 (2), 175–196.
Paul, B., 1968b. Macroscopic criteria for plastic flow and brittle fracture. In: In: Liebowitz, H. (Ed.), Fracture an Advanced Treatise, vol. II. Academic Press, New York, pp. 313–496.
Podgorski, J., 1985. General failure criterion for isotropic media. J. Eng. Mech. 111 (2), 188–201.
Priest, S.D., 2005. Determination of shear strength and three-dimensional yield strength for the Hoek-Brown criterion. Rock Mech. Rock Eng. 38 (4), 299–327.
Reches, Z.E., Dieterich, J.H., 1983. Faulting of rocks in three-dimensional strain fields I. Failure of rocks in polyaxial, servo-control experiments. Tectonophysics 95, 111–132.
Riedel, J.J., Labuz, J.F., 2007. Propagation of a shear band in sandstone. Int. J. Numer. Anal. Methods Geomech. 31 (11), 1281–1299.
Rubin, M.B., 1991. Simple, convenient isotropic failure surface. J. Eng. Mech. 117 (2), 348–369.
Rudnicki, J.W., 2017. A three invariant model of failure in true triaxial tests on Castlegate sandstone. Int. J. Rock Mech. Min. Sci. 97, 46–51.
Rukhaiyar, S., Samadhiya, N.K., 2017. A polyaxial strength model for intact sandstone based on artificial neural network. Int. J. Rock Mech. Min. Sci. 95, 26–47.
Runesson, K., Sture, S., Willam, K., 1988. Integration in computational plasticity. Comput. Struct. 30 (1), 119–130.
Schleicher, F., 1926. Der spannungszustand an der fliessgrenze (plastizitatsbedingung). Z. fur Angew. Math. Mech. 6 (3), 199–216.
Schreyer, H.L., 1989. Smooth limit surfaces for metals, concrete, and geotechnical materials. J. Eng. Mech. 115 (9), 1960–1975.
Schwartzkopff, A.K., Priest, S., Melkoumian, N., Egudo, A.J., 2013. Design and fabrication of a low cost true triaxial cell for testing multiple size specimens. In: Kwaśniewski, M., Li, X., Takahashi, M. (Eds.), True Triaxial Testing of Rocks. CRC Press/Balkema, The Netherlands, pp. 83–93.
Sloan, S.W., Booker, J.R., 1986. Removal of singularities in Tresca and Mohr-Coulomb yield functions. Commun. Appl. Numer. Methods 2, 173–179.
Stavropoulou, V.G., 1982. Behaviour of a brittle sandstone in plane-strain conditions. In: Proceedings of the 23rd US Symposium on Rock Mechanics, pp. 351–358.
Sture, S., Ko, H.Y., 1978. Strain-softening of brittle geologic materials. Int. J. Numer. Anal. Methods Geomech. 2 (3), 237–253.
Takahashi, M., Koide, H., 1989. Effect of the intermediate principal stress on strength and deformation behavior of sedimentary rocks at the depth shallower than 2000 m. In: Maury, V., Fourmaintraux, D. (Eds.), Rock at Great Depth, 1. Balkema, Rotterdam, pp. 19–26.
Tarokh, A., Li, Y., Labuz, J.F., 2017. Hardening of porous chalk from precompaction. Acta Geotech. 12 (4), 949–953.
Topping, A., 1955. The use of experimental constants in the application of theories of strength to rock. In: Proceedings Second Midwest Conference on Solid Mechanics, Purdue University, pp. 178–192.
Torre, G.D., 1949. Die grenzzustando statisch beanspruchter stoffe. Schweiz. Arch. Angew. Wiss u Tech. 15 (4,5), 116–145.
Vardoulakis, I., Goldscheider, M., 1981. Biaxial apparatus for testing shear bands in soils. In: Proceedings of the 10th International Conference on Soil Mechanics in Foundation Engineering, pp. 819–824.
Wawersik, W.R., Rudnicki, J.W., Olsson, W.A., Holcomb, D.J., Chau, K.T., 1990. Localization of deformation in brittle rock theoretical and laboratory investigations. In: Proceedings of International Conference on Micromechanics of Failure of Quasi-Brittle Materials, pp. 115–124.
Wawersik, W.R., Carlson, L.W., Holcomb, D.J., Williams, R.J., 1997. New method for true-triaxial rock testing. Int. J. Rock Mech. Min. Sci. 34 (3–4) 330.e1–330.e14.
Wiebols, G.A., Cook, N.G.W., 1968. An energy criterion for the strength of rock in polyaxial compression. Int. J. Rock Mech. Min. Sci. 5, 529–549.
Willam, K.J., Warnke, E.P., 1975. Constitutive model for the triaxial behavior of concrete. Proc. Int. Assoc. Bridge Struct. Eng. 19, 1–30.
Wong, T., Baud, P., 2012. The brittle-ductile transition in porous rock: a review. J. Struct. Geol. 44, 25–53.
You, M., 2009. True-triaxial strength criteria for rock. Int. J. Rock Mech. Min. Sci. 46 (1), 115–127.
Young, R.P., Nasseri, M.H.B., Lombos, L., 2013. Imaging the effect of the intermediate principal stress on strength, deformation and transport properties of rock using seismic methods. In: Kwasniewski, M., Li, X., Takahashi, M. (Eds.), True Triaxial Testing of Rocks. CRC Press/Balkema, The Netherlands, pp. 167–179.
Yu, M., 2002. Advances in strength theories for materials under complex stress state in the 20th century. Appl. Mech. Rev. 55 (3), 169–218.
Zeng, F., Li, Y., Labuz, J.F., 2018. Paul-Mohr-Coulomb failure criterion for geomaterials. J. Geotech. Geoenviron. Eng. 144 (2), 06017018. http://dx.doi.org/10.1061/(ASCE)GT.1943-5606.0001829.
Zhang, L., Zhu, H., 2007. Three-dimensional Hoek-Brown strength criterion for rocks. J. Geotech. Geoenviron Eng. 133 (9), 1128–1135.
Zhou, S., 1994. A program to model the initial shape and extent of borehole breakout. Comput. Geosci. 20 (7–8), 1143–1160.
Zimmerman, R.W., 1991. Compressibility of Sandstones. Elsevier Science.